



Basalt fibre reinforced geopolymer made from lunar regolith simulant

Final report

Authors: Anna-Lena Kjøniksen¹, Shima Pilehvar¹, Marlies Arnhof², Belinda Rich²

Affiliation: ¹Østfold University College, ²ESA ACT

Date: 30 September 2021

ACT research category: Space Architecture and Infrastructure (Habitats)

Contacts:

Anna-Lena Kjøniksen (Professor)

Department of Engineering, Østfold University College

P.O. Box 700, 1757 Halden, Norway

e-mail: anna.l.kjoniksen@hiof.no

Tel: +47 91991942

Leopold Summerer (Technical Officer)

Tel: +31(0)715654192

Fax: +31(0)715658018

e-mail: act@esa.int



Available on the ACT
website

<http://www.esa.int/act>

Ariadna ID: 18-9401

Ariadna study type: Standard

Contract Number: (4000125234/18/NL/GLC/as)

Table of Contents

Abstract.....	3
1. Introduction	4
2. Experimental program	5
2.1. Materials	5
2.1.1. Lunar regolith simulant	5
2.1.2. Alkaline solution.....	7
2.1.3. Basalt fibres.....	7
2.2. Geopolymer mixture design	9
2.2.1. Mix design and specimen preparation of geopolymer mixes made with different admixture types	9
2.2.2. Mix design and specimen preparation of geopolymer mixes made with different dosages of urea	11
2.2.3. Mix design and specimen preparation of geopolymer mixes reinforced with basalt fibre	11
2.3. Testing methods.....	11
2.3.1. Setting time	12
2.3.2. Shape deformation and layer-by-layer buildability	12
2.3.3. Compressive strength	12
2.3.4. Flexural strength	13
2.3.5. FTIR.....	13
2.3.6. X-ray tomography	13
2.3.7. Radiation testing - Neutron Irradiation.....	13
2.4. Vacuum 3D printing	15
3. Results and discussion.....	17
3.1. Setting time.....	17
3.2. Shape deformation and layer-by-layer buildability	18
3.3. Water reduction.....	21
3.4. Compressive strength of lunar geopolymer mixes made with different admixture types...	22
3.5. FTIR.....	23
3.6. X-Ray tomography.....	24
3.7. Compressive strength of basalt fibre-reinforced mixes.....	29
3.8. Flexural strength of basalt fibre-reinforced mixes	30
3.9. Radiation experiments.....	31
4. Conclusions	33
4.1. Future Work.....	34
References	34

Abstract

The presented Ariadna study investigates the additive manufacture of geopolymer using lunar regolith binder as a potential in-situ lunar construction technique. A recipe for geopolymer binders based on lunar regolith simulant was formulated and optimized in order to gain material properties suitable for lunar construction, while minimizing the use of water, and avoiding ingredients not available in situ (i.e. on the surface of the Moon). The addition of basalt fibres and superplasticizers to the recipe was evaluated. Based on an initial screening process, selected recipes were chosen for further testing. The effect of curing under simulated lunar environmental conditions (extreme temperature oscillations, vacuum) was investigated. The samples were tested for resistance to simulated lunar freeze thaw cycles, their suitability for basalt fibre reinforcement (to improve the material's tensile properties), and their neutron (secondary radiation) shielding capability. The suitability of the geopolymer recipes for 3D printing was evaluated and tested.

1. Introduction

Manufacturing and construction of extra-terrestrial infrastructure is a necessary step towards the sustainable human exploration of our solar system and beyond. It is envisioned that establishing a habitat on the lunar surface will facilitate surveys beyond lunar orbit [1]. However, the extreme environment presented on the lunar surface poses several challenges to survival, such as galactic and cosmic radiation, extreme temperature fluctuation, vacuum, meteoroids and lunar dust [2]. It is thus necessary to manufacture lunar habitats that can withstand these conditions while simultaneously protecting occupants and contents from their effects. There is motivation to construct these habitats using methods of In-Situ Resource Utilisation (ISRU), whereby the necessary materials are sourced from the lunar environment itself rather than launching from Earth. This significantly reduces the launch costs of the mission and makes construction of large scale, heavily shielded habitats feasible.

A number of ISRU construction techniques have been proposed previously. In particular, a number of techniques propose the manufacture of in-situ concretes and cementitious materials. Cesaretti et al. [3] proposed a D-shape 3D printing process with Sorel cement for construction on the lunar surface. Unfortunately, the process required substantial amounts of consumables (chemicals and water) to produce the binder. Buchner et al. [4] developed a rock-like material by using phosphoric acid as a liquid binder. For lunar applications, considerable amounts of water and phosphoric acid would have to be transported to the lunar surface. However, this material seems to be promising for use on the Martian surface, as phosphoric acid and water are available on Mars. Since water is a highly valuable resource on the lunar surface and not readily available [5], using building materials with high water demand is practically impossible. One alternative that requires no water to be produced is sulphur concrete, which could be manufactured on the lunar surface using sulphur extracted from troilite (FeS) [6]. However, sulphur concrete must be prepared under a narrow temperature range of 130–140 °C, has a maximum service temperature of 115 °C, and is highly prone to cracking under temperature cycling, making it impractical for use in the lunar environment [7]. Furthermore, sulphur cement materials exhibit lower radiation shielding than plain regolith alone [8].

Geopolymers are a class of cement-like materials which consist of silico-aluminates in an amorphous to semi-crystalline three-dimensional structure. They exhibit excellent properties such as quick controllable setting and hardening [9], [10], high compressive strength, freeze-thaw resistance [11], [12], excellent durability in sulfate environment and superior resistance to acid and salt attacks [13], [14], high fire resistance and low thermal conductivity [15], [16], low shrinkage [17] and adequate radiation shielding [18]. It has been proposed that lunar regolith be utilised as a precursor material to manufacture in-situ geopolymer, due to large amounts of aluminosilicates present in the regolith at a similar ratio to that of traditional geopolymer binders. Other materials required to produce geopolymers also have the potential to be sourced on the lunar surface: for example, alkali metals present in lunar regolith could be used as a source for the alkaline solution in the geopolymerisation reaction [19]. This means that, used in conjunction with large-scale 3D-printing technologies [20]–[22], geopolymers could be used to directly construct habitats and infrastructure using minimal resources launched from Earth and little-to-no human labour, the latter of which is crucial to minimising astronaut exposure and unnecessary extra-vehicular activity (EVA) [2].

To achieve the workability, shape retention, early strength and setting time required for 3D-printing [23], chemical admixtures can be added to the geopolymer mixture. Use of admixtures reduces the need to add additional water, which is less readily available on the moon [24] and reduces the compressive strength of the final material [25], in order to achieve desired workability. For terrestrial, fly ash-based geopolymers, a polycarboxylate-based superplasticizer is preferred when the calcium ion content is relatively high [26], while a naphthalene based superplasticizer is effective for low amounts of calcium [26], [27]. However, utilizing these superplasticizers in lunar geopolymers would involve transportation from the Earth at great cost. It is therefore preferable to find a superplasticizer that would be available on the moon. While the lunar surface is lacking in suitable materials for use as superplasticizers, we can also consider access to human waste materials if we

assume human presence during construction. Human urine contains approximately 9.3–23.3 g/L urea [28]. It is well known that urea is capable of breaking hydrogen bonds, thereby reducing the viscosities of many aqueous mixtures [29]. Thus, it is reasonable to assume that urea might work as a superplasticizer to reduce the water demand of geopolymers.

One method to maximise the mechanical properties of geopolymer structures is to reinforce with basalt fibre additions. Basalt fibres exhibit high strength and modulus, and excellent stability under high temperatures. Branston et al. [30] found that basalt fibre additions improved the first-cracking strength of Portland cement under flexural loading. Sufficient improvements, when applied to a lunar habitat scenario, would allow for more complex large geometries and structures. Basalt fibres could be produced in situ on the lunar surface by melting and extrusion of basalt rock, which has a melting point of approximately 1500 °C [31].

The objective of this study is fourfold: firstly, to develop a geopolymer recipe which effectively utilises urea as a chemical admixture to reduce water content while improving workability for 3D-printing; secondly, to characterise urea geopolymers in comparison with recipes traditional admixtures (polycarboxylate and naphthalene) in terms of their pre- and post-curing mechanical properties and morphology; thirdly, to investigate the effects of basalt fibre additions on urea geopolymers, including mechanical and radiation shielding properties of reinforced geopolymers; lastly, to develop a vacuum chamber extrusion assembly in order to properly evaluate the effects of the vacuum environment on 3D-printing of lunar geopolymers. The aim is to develop and verify a lunar regolith geopolymer mixture that can be successfully 3D-printed while meeting the severe curing conditions on the lunar surface (extreme temperature cycles, little available water, and vacuum), without the extreme cost of importing any material components from the Earth.

2. Experimental program

2.1. Materials

2.1.1. Lunar regolith simulant

In a lunar mission scenario, the lunar regolith is the most accessible and abundantly available *in-situ* resource. On Earth, geopolymer cements are commonly prepared using fly ash as a precursor, which bears a close compositional resemblance to lunar regolith as shown in Table 1. Accordingly, lunar regolith is the proposed geopolymer binder material for the preparation of lunar geopolymers. Due to the scarcity of real lunar material, investigations in this study were performed using a number of regolith simulants, namely DNA-1 and EAC-1A. JSC-1A was also initially chosen for investigation; however, due to limited availability this was not possible. The given simulants are formulated to imitate lunar soil samples retrieved in Apollo missions; their mineralogical compositions are also given in Table 1. Depending on the Si-Al ratio in a given precursor, the resultant geopolymer can take on different structures. Ratios > 3:1 create geopolymers that can be characterised as 2D networks, and ratios between 1:1 and 3:1 produce 3D polymeric networks. Lunar regolith exhibits the latter type Si-Al ratio necessary to produce geopolymer, with mare regolith exhibiting an Si-Al ratio of 2.6:1 and Highland regolith exhibiting an Si-Al ratio of 1.6:1.

Figure 1 shows micrograph images of fly ash and lunar regolith simulant DNA-1 under a scanning electron microscope (SEM). Due to environmental factors such as meteorite bombardment and the lack of natural erosion processes [32], lunar soils are angular, sharp and have a large particle size distribution, qualities which are reflected in the simulant soils. Fly ash, on the other hand, is generally spherical in shape and exhibits a smaller particle size distribution. Around 30% of the cumulative volume of regolith simulant particles overlap with the size range of fly ash, as determined by low angle laser light scattering (Figure 2). The two materials also vary in crystallinity: regolith simulant contains 75% crystalline phase, whereas fly ash contains 37% crystalline phase. It is anticipated that these differences in particle size and phase composition, alongside other factors such

as water content, could influence the geopolymerization reaction and final geopolymer structure. Accordingly, experimental work is required to optimise the lunar geopolymer recipe.

Table 1. Chemical composition of the three lunar regolith simulants and fly ash class F, compared to the composition of lunar regolith samples (the highest and lowest values of each component from 19 analyzed lunar samples is shown).

Chemical	Lunar regolith simulant DNA-1 (wt. %)	Lunar regolith simulant EAC-1A (wt. %)	Lunar regolith simulant JSC-1A (wt. %)	Fly ash class F (wt. %)	Lunar regolith soil samples range (wt. %)[33]
SiO ₂	47.79 ± 0.05	37.9±0.1	41.2±0.1	50.83 ± 0.04	40.6 - 48.1
Al ₂ O ₃	19.16 ± 0.07	11.91±0.06	17.01±0.07	23.15 ± 0.06	12.0 - 28.0
Fe ₂ O ₃	8.75 ± 0.01	16.65±0.01	17.11±0.01	6.82 ± 0.01	4.7 - 19.8
CaO	8.28 ± 0.03	12.92±0.03	12.66±0.03	6.87 ± 0.02	10.3 - 15.8
K ₂ O	3.52 ± 0.02	1.37±0.01	1.04±0.01	2.14 ± 0.01	0.04 - 0.55
Na ₂ O	4.38 ± 0.03	3.22±0.02	3.08±0.02	1.29 ± 0.01	0.31 - 0.70
MgO	1.86 ± 0.01	8.89±0.02	3.99±0.02	1.70 ± 0.01	5.6 - 13.0
TiO ₂	1.00 ± 0.01	2.58±0.02	2.32±0.01	1.01 ± 0.01	0.47 - 8.4

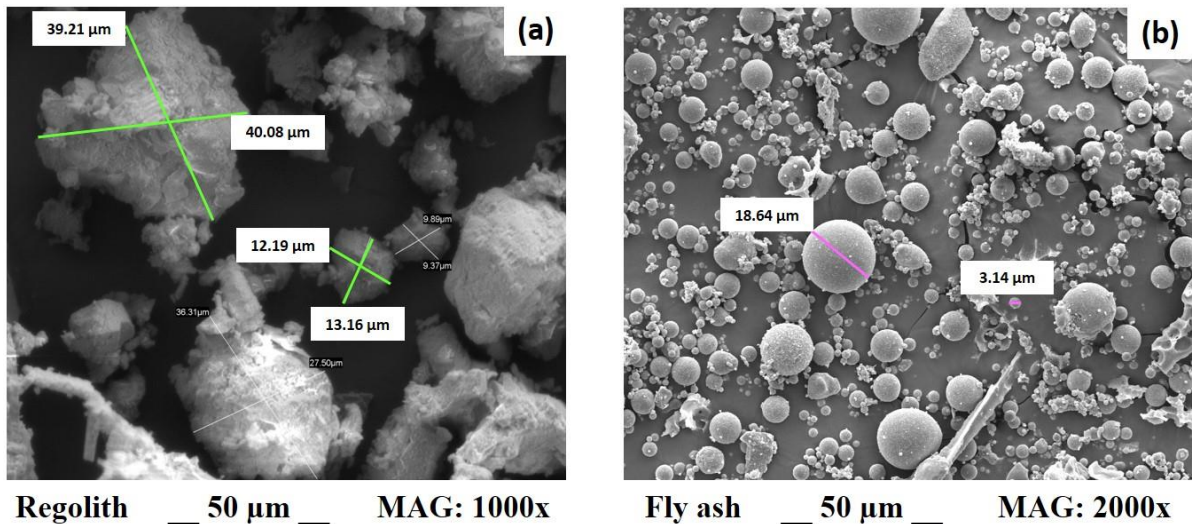


Figure 1. SEM images of (a) lunar regolith simulant DNA-1 and (b) fly ash.

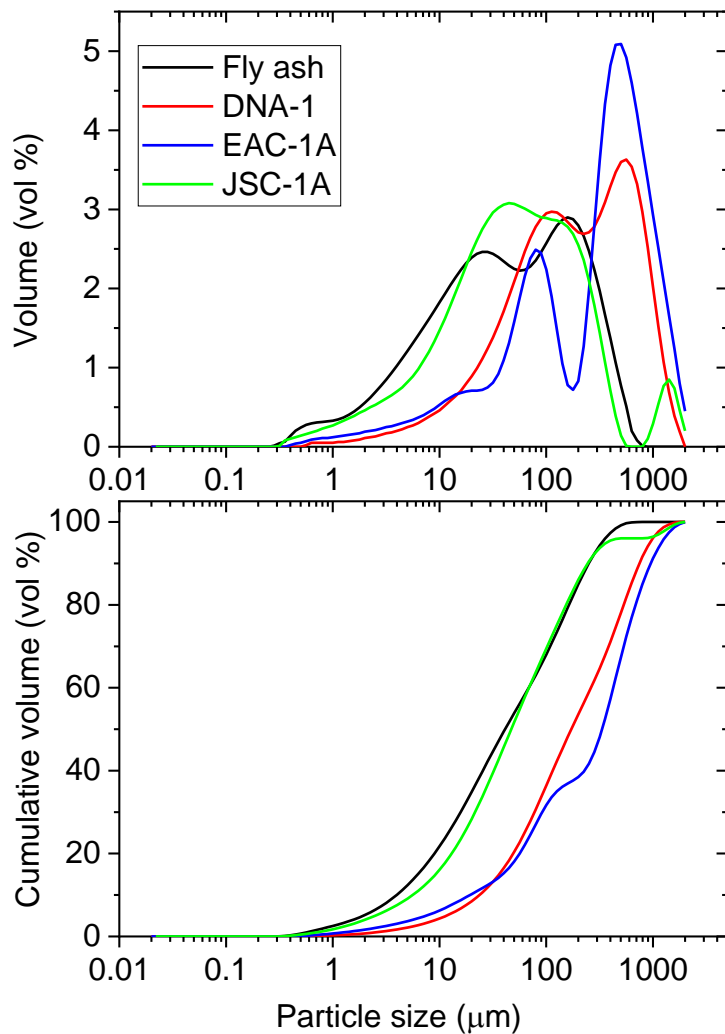


Figure 2. Particle size distributions of lunar regolith simulants and fly ash.

2.1.2. Alkaline solution

The alkaline solution used for the production of lunar geopolymer mixes consisted of a 12M NaOH solution. For this purpose, 480 g of NaOH pellets were dissolved in 1 L of distilled water. The solution was prepared one day in advance of making the mixes because the reaction between NaOH pellets and water is exothermic and releases heat. Therefore, the solution should be allowed to cool down before use.

2.1.3. Basalt fibres

Geopolymer can reach high compressive strength. However, as is the case with cementitious and ceramic materials in general, its flexural strength might be insufficient for large (tensile) structures [34]–[38]. To increase tensile capacity and ductility, the use of reinforcement fibres might be conducive. Ideally, these fibres would [31]:

- improve ductile capacity/tensile strength
- enhance resistance to fatigue and potential micrometeoroid impact
- limit crack size
- limit structural deformation

- avoid brittle failure at cracking

Building sizeable, fibre reinforced structures on the lunar surface calls for a fibre that is producible in situ.

Basaltic regolith is readily available on the Moon [39], [40], hence basalt fibres might present a favourable ISRU option for lunar reinforcement fibres [31]. Basalt fibre reinforcement has been used to improve the structural properties of geopolymer composites in terrestrial applications, exhibiting superior mechanical characteristics compared to pure geopolymers [41].

The fibres have advantageous biomechanical properties and could be sourced at the lunar surface by melting washed and crushed basalt rocks/regolith at approximately 1500 °C. Filaments would be produced by extruding the molten mass through nozzles. Such reinforcement fibres made from basalt could be shaped easily at will, spooled or chopped for further use. However, usually chopped strands of the basalt fibres are used for comparable terrestrial applications (i.e. concrete reinforcement).

The material exhibits the following beneficial characteristics:

- excellent stability
- high strength and elastic modulus
- high temperature resistance
- reduced thermal and electrical conductivity
- good chemical resistance (particularly in the presence of strong alkalis)
- non-toxicity
- comparatively easy manufacturing and handling

In the presented study, chopped basalt fibre strands (Basaltex, Belgium) in two different lengths (6.35 mm and 90 mm) were used in the production of lunar geopolymer samples. For comparative analysis, fibres with equal properties (e.g. diameter, density) were chosen. These properties are listed in Table 2 as provided by the manufacturer. The provided fibres were coated with a silane sizing (KV 12, KV 13 and KV 14). This organic polymer in water dispersion coating is necessary to stabilize the thread, secure flexible and resilient fibre properties and bonding between the basalt surface thread and the geopolymer matrix [42]. Due to polymer outgassing in ultra-high vacuum, the organic coating which is made for Earth applications is not suitable for use on the lunar surface [43]. Therefore, the fibre sizing was removed to increase the accuracy of the test results. Thermal treatment in a vacuum oven at 400°C was applied to the basalt threads for two hours. The recorded mass loss is 0.85 wt% for the 6.35 mm, and 0.51 wt% for the 90 mm long chopped fibres.

Table 2. Properties of basalt fibre [44].

Property	Reported value	Note
Diameter	17 µm	
Density	2.67 kg.dm ⁻³	
Moisture content	< 0.1 %	
Melting Temperature	1350 °C	
Tenacity (dry fibre)	> 600 mN/tex	ASTM D3822
Tensile Strength (impregnated fibre)	2.900 MPa	ASTM D2343
E-Modulus (impregnated fibre)	85 GPa	ASTM D2343
Melting Point	1350 °C	
Operating temperature	-260 °C to 600 °C	

Short term max. operation temperature	700 °C	
Fire blocker	Up to 1200 °C	
Coefficient of Thermal Expansion	1.4 x10 ⁻⁶ / °C	
Specific heat capacity	0.86 J.g ⁻¹ .K ⁻¹	(22 °C)

2.2. Geopolymer mixture design

2.2.1. Mix design and specimen preparation of geopolymer mixes made with different admixture types

A mixture design study was undertaken to determine an effective recipe for producing lunar geopolymer with superplasticiser additions. For lunar construction, it is necessary to develop a recipe which maximises desired material properties whilst minimising water content, due to scarcity, and chemical additions from Earth. Parameters investigated include alkaline solution chemistry, solution to binder ratio, admixture type, admixture percentage, setting temperature and binder particle size.

Regolith simulant DNA-1 was used as the geopolymer binder for the design of lunar geopolymer mixtures. The two alkaline solutions investigated were Na₂SiO₃ and NaOH. Initial tests with the Na₂SiO₃ solution found that a higher solution/binder ratio was required to achieve a workable mixture, due to high solution viscosity. Furthermore, recipes using Na₂SiO₃ did not set under room temperature during the 24h precuring time, which is attributed to not enough content of Na⁺ ions present in the solution to effectively contribute to geopolymerization.

NaOH solution provides a logistically better alternative for manufacturing geopolymer on the Moon, as the solution can be prepared from pellets using recycled water *in-situ*. A 12M NaOH solution was used to prepare lunar geopolymers with simulant and three different admixtures: naphthalene-based admixture FLUBE CR 100 F (henceforth referred to as N); polycarboxylate-based admixture SUPLA PDR 2 SA (henceforth referred to as C); and urea (henceforth referred to as U). A workable mixture was achievable using a NaOH/regolith binder ratio of 0.45 without admixture, or a ratio of 0.4 when 1 wt.% admixture (N, C or U) was added (where wt.% refers to weight percentage in relation to the regolith binder). The fresh mixtures exhibited too high viscosity and low workability required for 3D printing. It was also found that 24h setting time at room temperature was not sufficient for the samples to set properly; however, after being transferred to an 80°C incubator for 24h the samples were set and could be demoulded. Accordingly, a high temperature setting stage is desirable for these materials. Considering the temperature variations on the moon (Figure 3), this suggest that the lunar day-time is best suited for 3D-printing the geopolymers.

To address the problem of high mixture viscosity, the admixture content was increased to 2 wt.% to increase workability while avoiding additional water content. The same NaOH/regolith binder ratio (0.4) was kept and mixtures were prepared using 3 wt.% N, C and U admixtures, as well as mixture without. Better workability and lower porosity were achieved with increased admixture for all recipes. However, after precuring for 24h at 80°C samples with N additions were still soft and prone to breakage during demoulding. Some U samples exhibited cracking during the precuring stage itself, attributed to gas generated at high temperature unable to escape the rigid mould. The C mixture proved the most viscous of the three, and produced precured samples with the highest strength and most uniform structure. However, samples are too stiff for casting and printing, causing the formation of heterogeneous and fractured structures.

The final part of the mixture design stage investigated the effect of regolith particle size on workability, water content requirement and setting time. DNA-1 regolith was sieved to separate fine and coarse particles, with fine being considered the ≤ 75 μm fraction and all larger particles being considered the coarse fraction. Based on the previous result, polycarboxylate (C) type admixture was chosen to be added in 2 wt.% quantity. Varying ratios of coarse/fine regolith were investigated to find the required NaOH/regolith ratio. Samples made with fine regolith alone required a solution/binder

ratio of 0.4, as did samples made with 50% fine and 50% coarse regolith. Samples with 35% fine regolith (65% coarse) required 0.35 solution/binder ratio, as did samples with 30% fine regolith (70% coarse). Thus, increasing coarse regolith content reduces the solution/binder ratio, and therefore reduces the required water content. However, after 24h precuring at 80°C the samples with higher coarse content exhibited greater numbers of air voids and higher porosity, due to lack of infill from finer particles. The ideal fine/coarse ratio was selected to be 50/50 – this is a reduced number of coarse particles compared to the as-received simulant, which showed a 40/60 fine to coarse ratio.

From all above investigations and laboratory trials of workability and buildability, it has been shown that an alkaline solution to regolith ratio of 0.35 and a chemical admixture dosage corresponding to 3% of the lunar regolith mass were optimal. Table 3 lists the final mixtures selected to be viable. For mixing, the regolith, alkaline solution, and admixture in each case were mixed for 10 min and then cast into 3 × 3 × 3 cm³ moulds. Vibration was used for 1 min to remove trapped air before precuring specimens at 80 °C for 6 h. Once demoulded, samples were exposed to freeze-thaw cycles. A heating chamber was used to exposed them to temperatures of 80 ± 2 °C for 48h, followed by being placed in a freezer at -80 ± 2 °C for 48h.

Table 3. Mix design of lunar geopolymers made with different chemical admixtures.

Mix	Alkaline solution/Regolith	Chemical admixture
W/O	0.35	–
U	0.35	Urea – 3%
C	0.35	polycarboxylate based (SUPLA PDP 2 SA) - 3%
N	0.35	naphthalene based (FLUBE CR 100 F) - 3%

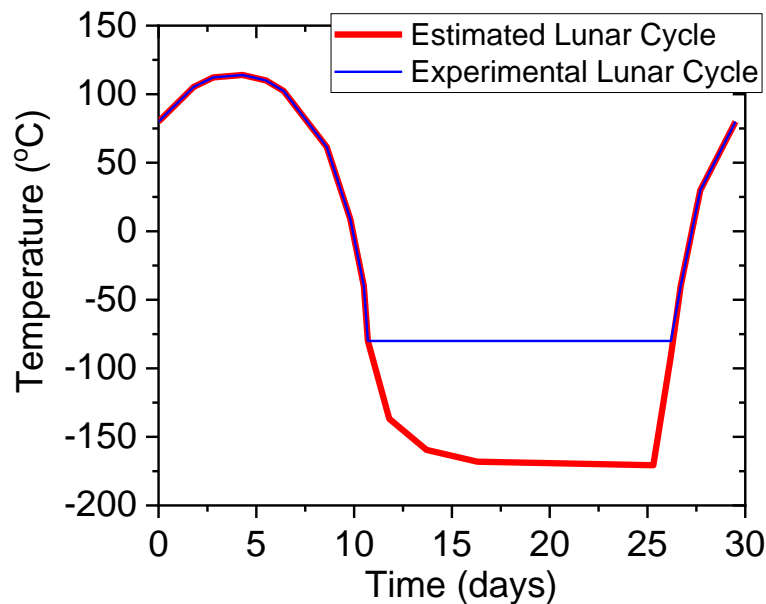


Figure 3. Estimated lunar temperature variation [45], and the experimental lunar cycle utilized in this work (limited due to lack of sub -80 °C freezer).

2.2.2. Mix design and specimen preparation of geopolymer mixes made with different dosages of urea

In order to evaluate the effect of different contents of urea on the performance of lunar geopolymer mixes under severe lunar conditions, three different urea dosages including 0%, 3%, and 5% of the binder content were selected. Note that these mixes were prepared with the optimal alkaline solution to regolith ratio of 0.35. Furthermore, mixes with the same workability were produced by adjusting the alkaline solution to regolith ratio in order to gain insights into the water reduction achieved by using urea as superplasticizer. The mix proportioning is shown in Table 4.

Table 4. Mix design of lunar geopolymer mixes with different urea content.

Mix	Lunar regolith (g)	Water (g)	NaOH pellets (g)	Urea (g)	Alkaline solution/Regolith ratio	Water/Solid ratio
LG0W	1000	288	162	0	0.45	0.25
LG3W	1000	224	126	30	0.35	0.19
LG5W	1000	205	115	50	0.32	0.17
LG0	1000	224	126	0	0.35	0.2
LG3	1000	224	126	30	0.35	0.19
LG5	1000	224	126	50	0.35	0.19

For specimen preparation, regolith and alkaline solution were mixed with urea together for 8 min to obtain a homogenous mix. Afterwards, the fresh paste was poured into cube samples with side length of 40 mm. The compaction of samples was done by using a vibration machine for 1 min. After that, samples were divided into two groups: one group was pre-cured in a vacuum thermal chamber (Binder VD23 Vacuum Oven) at 0.01 mbar at 80 °C for 3 h, while the other group was pre-cured in an ambient thermal chamber at 80 °C for 3 h. Then, the samples were demolded and subjected to a lunar cycle in vacuum environment as shown in Figure 3.

2.2.3. Mix design and specimen preparation of geopolymer mixes reinforced with basalt fibre

The effect of basalt fibre addition on the performance of lunar geopolymer mixes was investigated by applying 1% basalt fibre (by total mass of the mix) with two different lengths. The short basalt fibre, here forth referred to as SBF, had a length of 6.35 mm and the long basalt fibre, here forth referred to as LBF, had a length of 90 mm. The alkaline solution to regolith (EAC type) ratio and urea content were kept constant at 0.3 and 2% of regolith weight, respectively, for all mixes.

A mixing process similar to that presented in the previous sections was adopted for making basalt-fibre reinforced geopolymer mixes. The fibers was added to the dry materials before mixing with alkaline solution.

The fresh mix was poured into cube samples with side length of 50 mm and beam samples with 160 mm × 40 mm × 40 mm. The samples were pre-cured in both ambient and vacuum conditions for 24 h at 80 °C. Then, the samples were demolded and cured in lunar conditions described earlier.

2.3. Testing methods

The following experiments were carried out to characterise the properties of the lunar geopolymer both before and after curing. These characterisations were performed to compare the effects of each admixture addition, i.e. polycarboxylate (C), naphthalene (N), urea (U) and without

admixture (W/O). Unless otherwise stated, only these additions differed between samples and all other casting/curing parameters remained the same.

2.3.1. Setting time

Initial and final setting time were characterised for all lunar geopolymer samples after mixing and casting into moulds. A Vicat needle test was performed with a manual Vicat needle apparatus in accordance with EN 196-3. Setting time measurements were carried out during the precuring stage at 80°C with an interval of 15 min. The initial setting time was given to be the time at which needle penetration is less than 39 mm, whereas final setting time was given to be the time at which needle penetration depth is 0.5 mm.

2.3.2. Shape deformation and layer-by-layer buildability

Shape deformation is a measure of the shape retention of the geopolymer after demoulding and before pre-curing. This is a particularly important attribute of the material during extrusion 3D printing. Fresh samples were prepared for each geopolymer/admixture combination using 200 g of mixture in a conical mould. Immediately after demoulding, 1 kg and 2 kg weights were placed atop the fresh samples. The percentage shape deformation under pressure was calculated as follows:

$$\text{Shape deformation} = \frac{D_{\text{after}} - D_{\text{before}}}{D_{\text{before}}} \times 100 \quad (1)$$

where D_{before} and D_{after} are the bottom diameter of the sample before and after demoulding, respectively. The value of D_{before} is set by the internal diameter of the bottom of the mould and is given to be 70 mm for all samples.

After evaluating shape deformation, mixtures with the highest shape retention and usable workability were selected to be tested for layer-by-layer buildability. A high-pressure syringe pump (Fusion 6000, Chemyx Inc.) with constant pump rate of 20 ml/min was used to extrude multiple layers of fresh geopolymer mixture (Figure 4). The buildability was assessed by visual inspection.



Figure 4. A high-pressure syringe pump is utilized for 3D-printing the samples.

2.3.3. Compressive strength

The compressive strength tests for lunar geopolymer specimens after 0, 2, 4 and 8 freeze-thaw cycles were performed at 20 °C in accordance with EN 12190, using a digital compressive strength test machine (Form Test Machine).

2.3.4. Flexural strength

A three-point flexural test was conducted on beam specimens with dimensions of 160 mm × 40 mm × 40 mm at 20 °C based on the guidelines of EN 12390 by using a digital flexural strength test machine.

2.3.5. FTIR

Lunar geopolymer specimens were characterized via Fourier-Transform Infrared Spectroscopy (FTIR) after 0, 4 and 8 freeze-thaw cycles. FTIR analysis was conducted with a spectrometer (PerkinElmer Spectrum BX) in transmittance mode from 4000 to 500 cm⁻¹. Samples were dried before measurement by placing in a heating chamber at 80 °C for 12 h.

2.3.6. X-ray tomography

X-ray microtomography (XCT) was used to characterise the effect of different admixtures on specimen porosity and micro-crack formation under freeze-thaw cycling. Scans were performed on drill cores of samples before and after exposure to four freeze-thaw cycles. The cylindrical cored samples had a diameter of 10 mm and a height of approximately 20 mm. Analyses were performed using a Skyscan 1172 XCT scanner, with an energy of 100 kV, 0.9 s acquisition time and 0.3 rotation step. Tomographic reconstruction was performed using the FDK algorithm [46]. The reconstructed images consist of 1200 vertically stacked cross-sections, with a linear pixel size of 6.5 mm. Image processing, including binary segmentation and particle analysis, was performed using the ImageJ software [47], by which the size of non-interconnected pores was measured. In order to estimate the accuracy and error associated with the image processing procedure, a random distribution of spherical pores with known particle size was generated. After addition of gaussian noise, the image was binarized and the total porosity and sphere radius was compared with those relative to the original image. The average errors associated with porosity and pore radius were 4% and 15% respectively.

2.3.7. Radiation testing - Neutron Irradiation

The radiation shielding properties of geopolymer are an important point of interest in the context of space infrastructure. In the lunar environment, the lack of atmospheric shielding means surface missions experience high-level exposure to ionising radiation from galactic cosmic rays and solar particle events. This represents a major hazard of human lunar exploration, due to the negative medical effects of radiation exposure. Moreover, scientific equipment employed on the lunar surface is also vulnerable to radiation, as ionising particles can cause computational errors or accelerated material degradation. The presence of significant shielding material can prevent these radiation effects and reduce the radiation level to within the permissible daily dose.

Neutron irradiation experiments were carried out to compare the shielding efficiency of lunar geopolymers with previous studies on sintered lunar regolith [48], [49]. The experiments were carried out at the ChipIR facility at the STFC ISIS Neutron and Muon Source, Harwell, UK. Geopolymer samples for irradiation were prepared from DNA-1 lunar regolith simulant, sodium hydroxide and urea, as 30 × 30 × 30 mm³ cubes. The cubes were wrapped in foil to prevent spread of contaminated particles post-irradiation. The effects of aluminium foil, with thickness approximately 0.025 mm, on neutron transmission were considered negligible.



Figure 5. Experimental setup for ChipIR experiments. Four samples are arranged in a dedicated sample holder, courtesy of A. Meurisse. The green laser light indicates the path of the neutron beam. Detectors to measure transmission are placed before (not shown) and after (visible on the right-hand side panel) the samples.

Four types of sample were prepared: two sets were cured under ambient conditions, and two sets were cured under vacuum. Within each set, half were prepared with 1% chopped basalt fibre reinforcement, and half were prepared without. Samples were placed in a sample holder to align them with the beam in such a way that multiple cubes of the same type could be stacked, as shown in Figure 5. Figure 5. Experimental setup for ChipIR experiments. Four samples are arranged in a dedicated sample holder, courtesy of A. Meurisse. The green laser light indicates the path of the neutron beam. Detectors to measure transmission are placed before (not shown) and after (visible on the right-hand side panel) the samples. By stacking 30 mm cubes in succession, transmission measurements were taken at a series of thicknesses, i.e., 30 mm, 60 mm, 90 mm and 120 mm. Silicon detectors were placed before and after the sample holder to determine transmission through the sample, and each experiment ran for 1 hour. Measurements were also taken with no sample present as a control. Table 5 shows the test schedule for irradiation experiments, including the four types of sample prepared for irradiation.

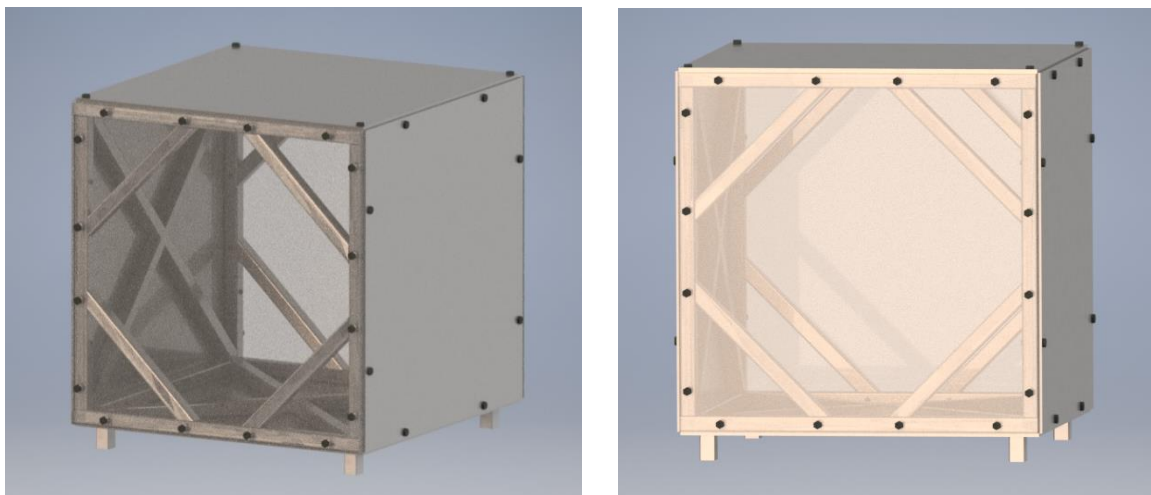
Table 5. Sample test schedule for basalt fibre reinforced geopolymer samples.

Test No.	Sample	Chopped basalt fibre reinforcement	Curing conditions	Thickness
0	Blank measurement No. 1			
1				30 mm
2	V0	0 %	Vacuum	60 mm
3				90 mm
4				120 mm
5	V1	1 %	Vacuum	30 mm

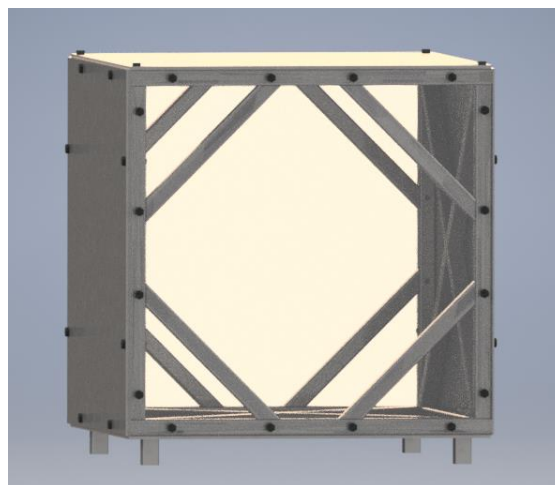
6				60 mm
7				90 mm
8				120 mm
9	Blank measurement No. 2			
10				30 mm
11	A0	0 %	Ambient	60 mm
12				90 mm
13				120 mm
14				30 mm
15	A1	1 %	Ambient	60 mm
16				90 mm
17				120 mm

2.4. Vacuum 3D printing

In order to simulate 3D printing on the surface of the moon, a vacuum chamber was designed and included in the 3D printer model used for concrete printing. The chamber is placed in frame, which is shown in **Error! Reference source not found.**. The dimensions an

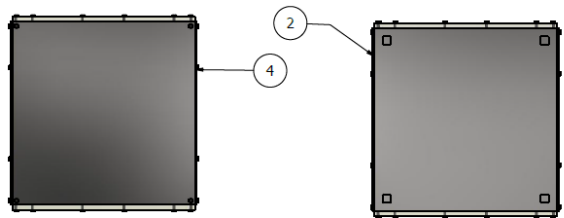
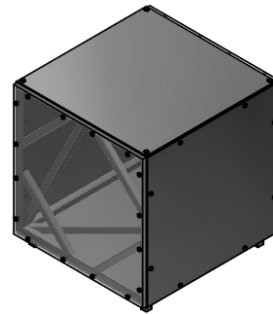
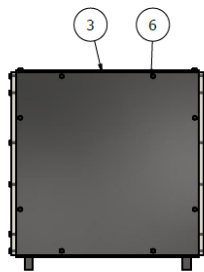
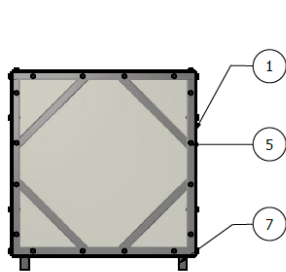


d the information about the printer features the positioning of the dimensions – these can **Reference source not**



the different parts of the 7. Within the chamber, actuators which control extruder nozzle in three be seen in Figure 8**Error! found..**

Figure 6. Frame supporting the vacuum chamber.



PARTS LIST			
ITEM	QTY	PART NUMBER	DESCRIPTION
1	2	PCplate	
2	1	Stålplate	
3	2	Stålplate_side	
4	1	Stålplate_topp	
5	32	ISO 4016 - M16 x 80	Hexagon head bolts. Product grade C
6	20	ISO 4016 - M16 x 65	Hexagon head bolts. Product grade C
7	4	Bein	

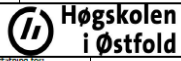
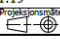
Dato: 28.09.2021	Konstr./ tegnet: olepm	Målestokk: 1:19	 Høgskolen i Østfold
Inventor 2021		 <small>Prosjeksjonsmåte</small>	
Henvisning/tittel: Vakuukkammerv2		<small>Erstatning for:</small>	

Figure 7. Part list and dimensions of the frame.



Figure 8. Internal view of the chamber frame with two pneumatic actuators visible.

3. Results and discussion

3.1. Setting time

Figure 9 shows the effect of different superplasticizers on the initial and final setting times of lunar geopolymer at 80 °C. The three superplasticizers influence the setting times in different ways. Incorporating 3% urea (U) postpones both initial and final setting times in comparison with the sample without any chemical admixture (W/O). For both mixtures containing 3% polycarboxylate-based admixture (C) and naphthalene-based admixture (N), there is a moderate delay of the initial setting time, while a much longer final setting time was observed for the N mixture. In 3D printing, the time after mixing until the fresh material loses the workability for extruding is called the open time. The open time is always earlier than the initial setting time [50]. Therefore, a longer initial setting time will help maintain a continuous flow during pumping, and prevent the material from becoming too hard in the 3D printer. For good shape retention during layer-wise construction, the fresh geopolymer mixture should gain high early strength after extrusion to tolerate subsequent layers resting on top [22]. Acceptable final setting time is therefore an advantage to allow the LG layers to be loaded onto the previous layers without shape deformation. Accordingly, the mixture containing urea exhibits the best initial and final setting times for 3D printing.

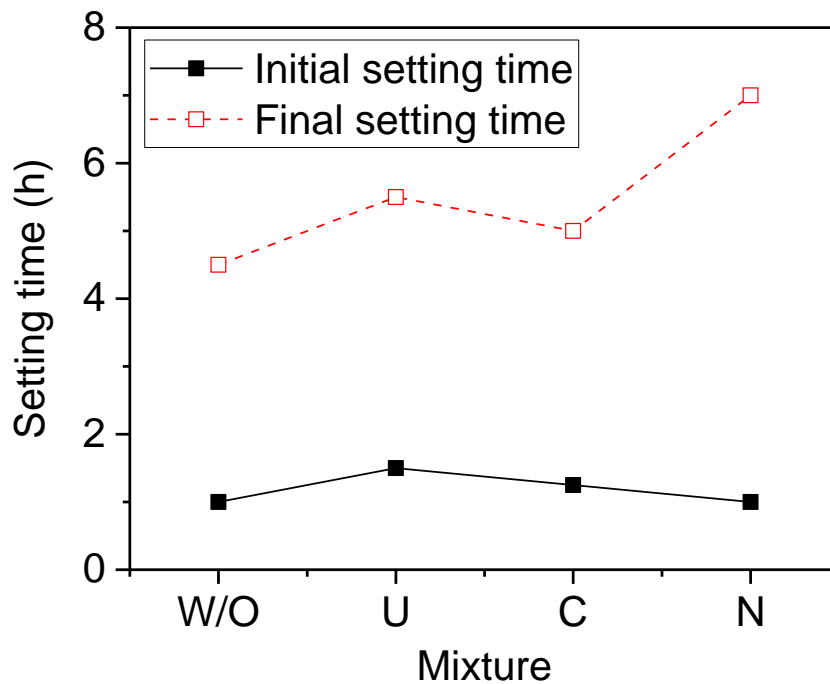


Figure 9. The initial and final setting times of W/O (without any admixture), U (urea), C (polycarboxylate-based admixture) and N (naphthalene-based admixture) lunar geopolymer mixtures.

3.2. Shape deformation and layer-by-layer buildability

One of the greater challenges in 3D concrete printing is that the materials should be able to retain their shape after extruding. **Error! Reference source not found.** depicts shape deformation of fresh mixtures after placing a 1 kg weight on top of the samples. As can be seen from **Error! Reference source not found.**a and c, fresh W/O and C samples retain a stable shape after loading with a 1 kg weight. However, there are many fractures in the samples, due to the stiffness of the mixtures during mixing and moulding. To have a low shape deformation, a mixture should have a good workability and high viscosity. However, the W/O and C samples are too stiff for casting, causing the formation of heterogeneous and fractured structures. It has previously been shown that a polycarboxylate-based superplasticizer (such as the one used in sample C) is often the best choice for fly ash class C, due to the strong bonds between the positively charged calcium and the negatively charged polycarboxylate [26]. Since the lunar regolith simulant is similar to fly ash class F, this superplasticizer is not optimal for improving the workability and flowability of the mixture. From **Error! Reference source not found.**b and d it is evident that fresh U and N mixtures are castable after moulding and exhibit smooth surfaces with none (U sample) or few (N sample) fractures. These samples also retain their shape under a 1 kg external load. Accordingly, mixture U and N were selected for further studies.

In the next step, a 2 kg weight was placed on top of the fresh U and N mixtures for shape deformation evaluation (Figure 11). The percentage of shape deformation was 11.4% and 13% for the U and N mixtures, respectively. Thus, the sample containing urea retains its shape better than the other specimens investigated after loading with a weight that is 10 times that of the 200 g sample.

In Figure 12, layer-by-layer buildability was measured by means of a syringe pump for selected mixtures (U and N) to see how many layers is possible to stack without any deformation of the layers or collapse of the structure, and without utilizing a rest time between layers. Due to the narrow extruding tube (10 mm in diameter), only 4 and 5 layers of filament were built up for the U and N samples, respectively. As can be seen from Figure 12, there are slight changes of the thickness of each layer. However, all the layers are nicely vertically stacked, and remain steady without any obvious

deformation and collapse. Accordingly, urea and the naphthalene-based admixture can contribute positively to the buildability of the lunar geopolymer. Furthermore, **Error! Reference source not found.** shows the layer-by-layer buildability of geopolymer mixes with urea content of 3% and 5%. Similarly, the layers were made by a syringe pump, and it is seen that mix with urea content of 3% showed a superior buildability compared to mix with 5% urea content. It confirms that the optimum amount of urea to be used in the production of 3D printed geopolymer mixes is 3%.

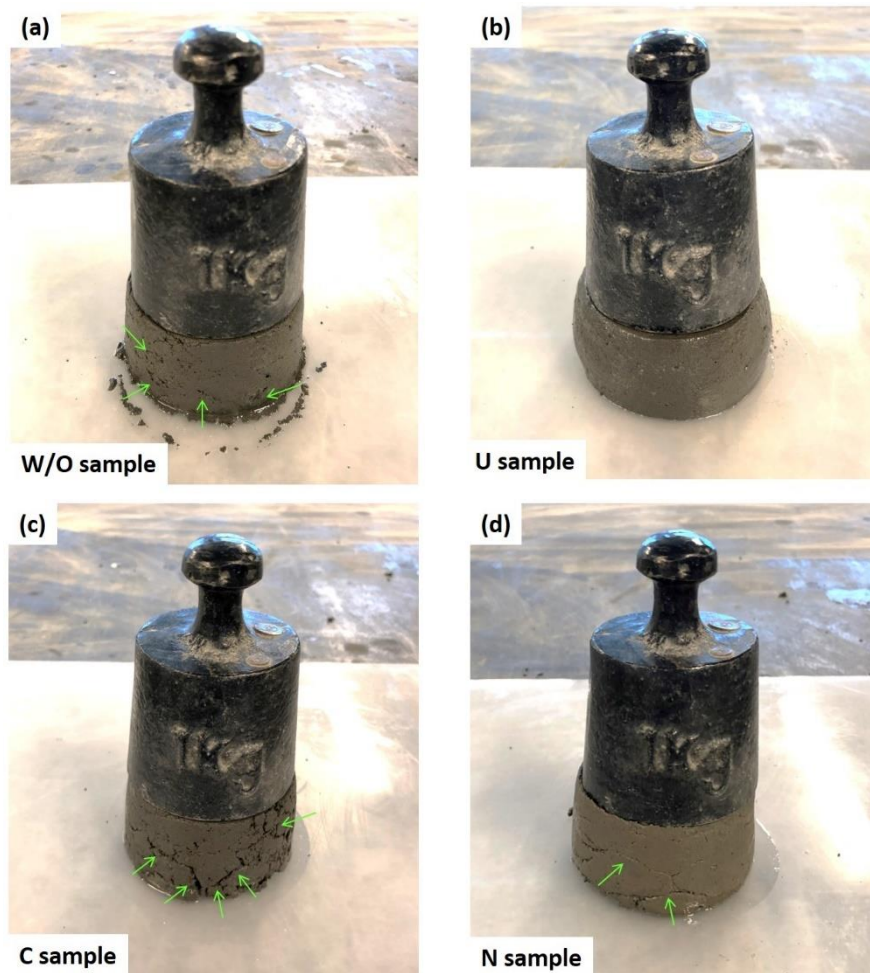


Figure 10. Sample retention after loading a 1 kg weight over (a) mixture without any admixture (W/O sample), (b) mixture containing 3% urea (U sample), (c) mixture containing 3% polycarboxylate-based admixture (C sample), and (d) and mixture containing 3% naphthalene-based admixture (N sample). The arrows show fractures and disruptions formed during molding.

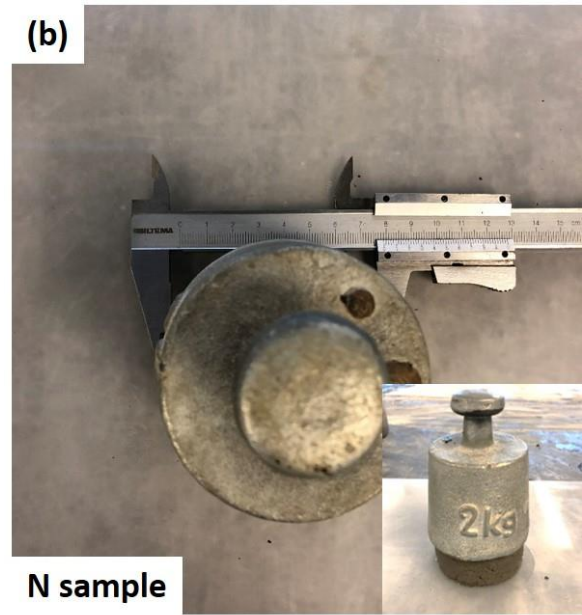
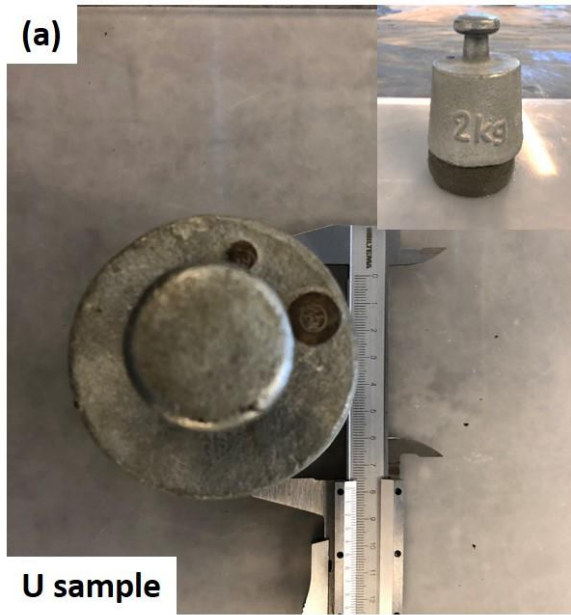


Figure 11. Sample deformation after loading a 2 kg weight over (a) mixture containing 3% urea (U sample), (b) mixture containing 3% naphthalene-based admixture (N sample).



Figure 12. Layer-by-layer buildability of (a) mixture containing 3% urea (U sample), (b) mixture containing 3% naphthalene-based admixture (N sample).

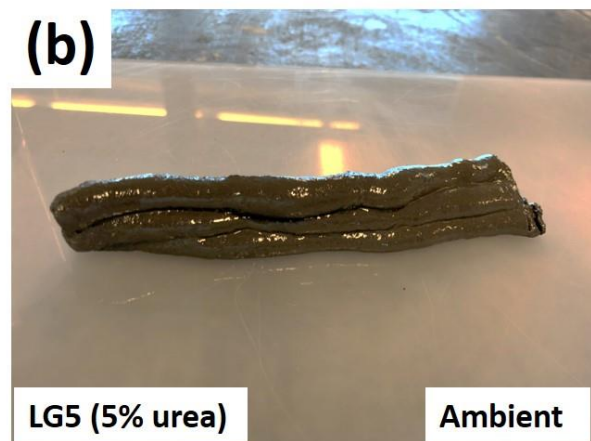
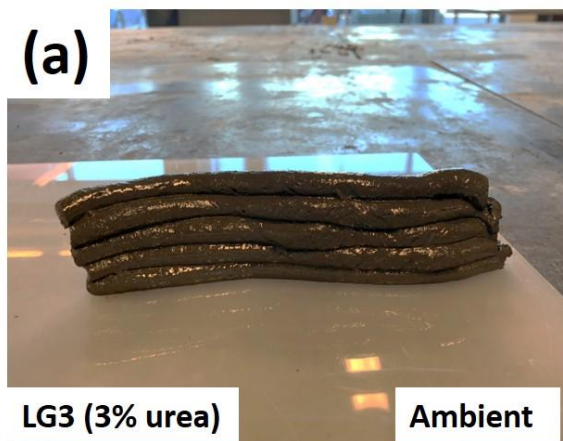


Figure 13. Buildability of (a) mixture containing 3% urea (LG3) and (b) mixture containing 5% urea (LG5) at ambient conditions. Extruded through a 1 cm tube.

3.3. Water reduction

Due to the limited access of water on the moon, it is essential to keep the water content in the LG mixture as low as possible while retaining sufficient workability and strength. Mini slump experiments were utilized to quantify the reduced amount of water needed to retain the same workability in the presence of urea. A flow table with a cone (diameter of 10.16 cm at the base and 6.09 cm at the top) was utilized, and each sample was dropped 25 times before measuring the sample diameter as illustrated in Figure 14. The reduced water demand in the presence of urea was determined by comparing the amount of water needed to reach a fixed diameter deviation of 0.5 cm between the diameter of the sample and the base diameter of the cone.

The water to geopolymer solids ratio needed to reach the same diameter deviation (0.5 cm) of the mini slump experiments for mixtures containing 0 (LG0W), 3 (LG3W), and 5 (LG5W) wt. % urea, is shown in Figure 15a. Increasing the amount of urea from 0 to 5 wt. %, reduced the water demand by 32 % (Figure 15b). As can be seen from Figure 14, LG0 has visible cracks and low consistency, although the flowability was the same as the other samples. Urea can break hydrogen bonds [51]. The addition of urea to the geopolymers can therefore reduce the amount of water needed to achieve a good workability of the samples [52], which is critical for construction on the moon.

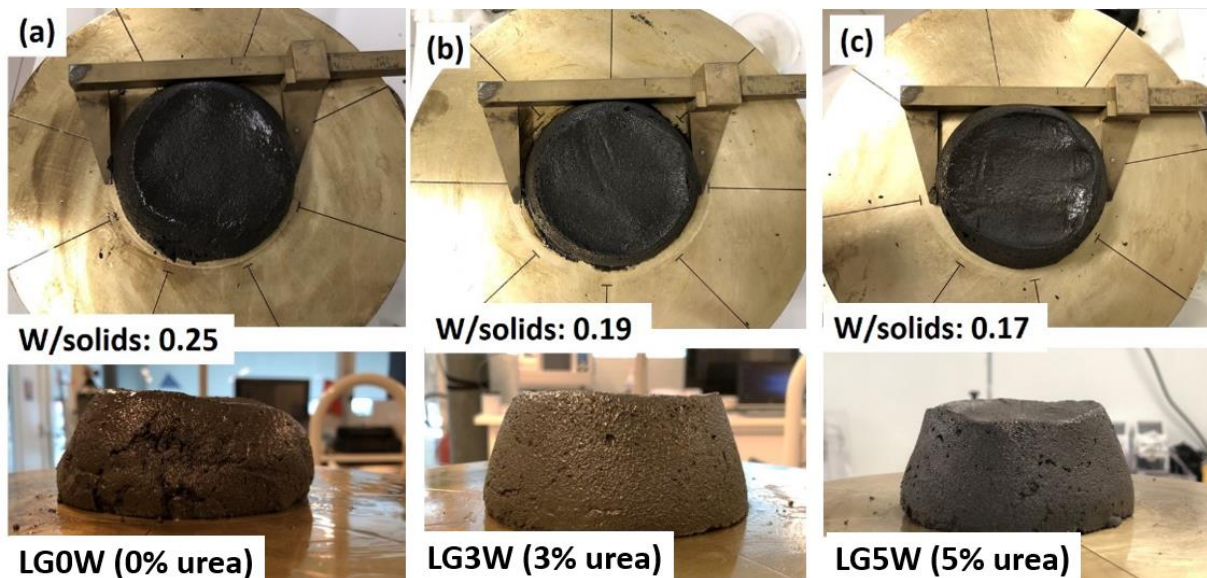


Figure 14. Mini slump measurements of the flowability of the geopolymers. To retain the same workability in all mixtures, the water to solids ratio has been varied. a) Without urea, water to solid ratio = 0.25, b) 3 % urea with respect to regolith, water to solid ratio = 0.19, c) 5 % urea with respect to regolith, water to solid ratio = 0.17.

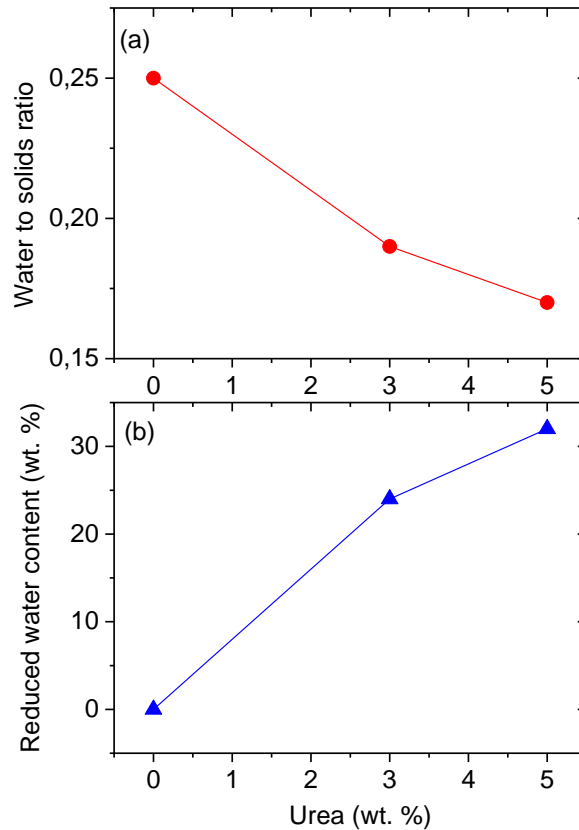


Figure 15. (a) The water to geopolymer solids ratio needed to obtain a constant mini slump at different urea concentrations, (b) reduced water content compared to the sample without urea.

3.4. Compressive strength of lunar geopolymer mixes made with different admixture types

The compressive strength of the samples after 0, 2, 4 and 8 freeze-thaw cycles is shown in Figure 16. The sample without any chemical admixture exhibits the highest compressive strength after 8 freeze-thaw cycles (32 MPa). As mentioned previously, 3D printing requires high early strength after extrusion to tolerate the weight of subsequent layers loaded on top of the sample. The C and N samples show a low early strength of about 1.7 MPa, which is not optimal for 3D printing. Interestingly, the U sample exhibited a relatively high initial compressive strength (13 MPa) after precuring at 80 °C.

During the freeze-thaw cycles, two opposing mechanisms are affecting the compressive strength. The freeze thaw cycles are expected to reduce the compressive strength due to expansion of water within the samples when it freezes, which may cause fractures within the specimen. At the same time, the geopolymerization reaction within the samples continues, which will increase the compressive strength. This results in a continuous slight increase in compressive strength for the U sample. For the three other samples the competing mechanisms causes a variation in compressive strength over the freeze thaw cycles, but with an overall strong increase from 0 to 8 cycles. The compressive strength requirement for lunar construction is 1/6 of the requirement of a similar structure on Earth [18], which is normally around 25–40 MPa [53]. Except for the C and N samples before the freeze-thaw cycles, all samples are well above this limit (>7 MPa).

After 8 freeze-thaw cycles, the U and N samples have approximately the same compressive strength, while the sample without superplasticizer has a much higher compressive strength. The C sample has a large variation between the three tested cubes, but seems to have a strength somewhere between the other samples. Interestingly, the samples with the lowest compressive strength after 8

freeze-thaw cycles (U and N) are the same ones that are best suited for 3D printing (**Error! Reference source not found.**, Figure 12). In order to explore the mechanisms behind the differences, FTIR and X-ray microtomography experiments have been performed.

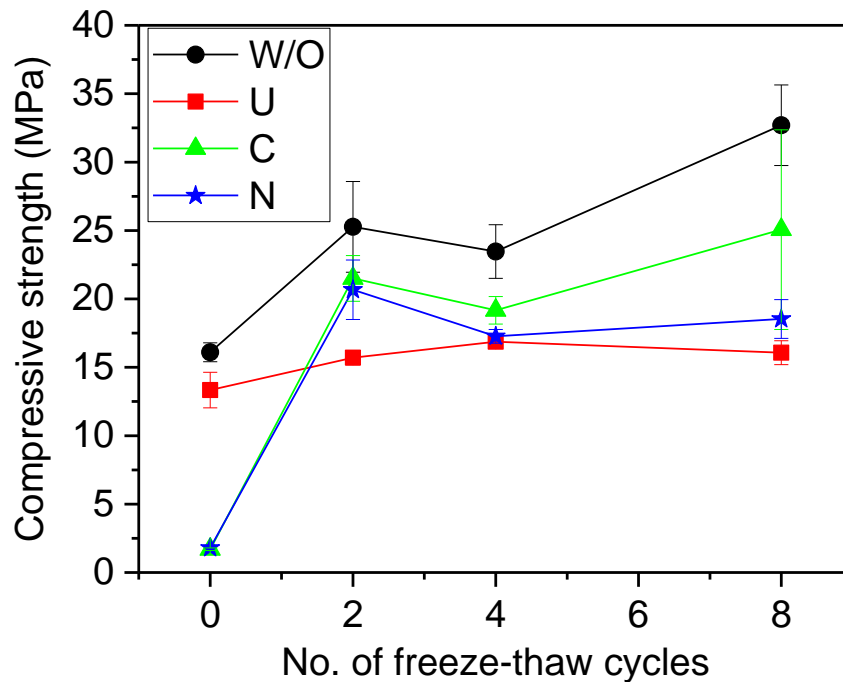


Figure 16. Compressive strength of lunar geopolymer versus the number of freeze-thaw cycles containing 0 wt.% of superplasticizer (W/O) and 3 wt.% of urea (U), 3% polycarboxylate-based admixture (C), and 3% naphthalene-based admixture (N). The samples were pre-cured for 6 h at 80 °C before starting the freeze-thaw cycles.

3.5. FTIR

Figure 17 presents the FTIR spectra of the four different geopolymers after 0, 4, and 8 freeze-thaw cycles. The main band is centered around 975 cm^{-1} and corresponds to asymmetric stretching vibration of Si—O—T (where T = Si or Al) [13-15]. This peak indicates the degree of amorphous aluminosilicate gel phase due to dissolution of the regolith in the alkaline solution [54]. After 0 freeze-thaw cycles, this peak is strongest for the W/O and U samples, which is in agreement with the higher compressive strengths of these samples at this stage (Figure 16). After 4 freeze-thaw cycles (Figure 17b), the C sample exhibited the highest amount of geopolymer gel formation resulting in a broader and deeper peak. In contrast, the sample containing urea (U) exhibited the smallest amount of gel which resulted in the lowest compressive strength after 4 freeze-thaw cycles (Figure 16). Interestingly, after 8 freeze-thaw cycles, the U sample revealed similar intensity and depth of this peak as the C sample, which indicates a continuing formation of geopolymeric products after 8 freeze-thaw cycles.

The broad IR band at around 2358 cm^{-1} (after 4 and 8 freeze thaw cycles) is related to the bending vibration of H—O—H bonds from weakly bound water molecules [54]. Since this peak is not evident before the freeze-thaw cycles, this is probably from water adsorbed onto the samples during the freeze-thaw process.

The small peaks at 1428 cm^{-1} have been attributed to stretching vibrations of O—C—O bonds, which suggests that sodium bicarbonate has been formed due to atmospheric carbonation of the high alkaline NaOH solution [54]. There are a number of smaller peaks in the $630\text{--}760\text{ cm}^{-1}$ region, which are attributed to aluminosilicate ring and cage structures [55], [56].

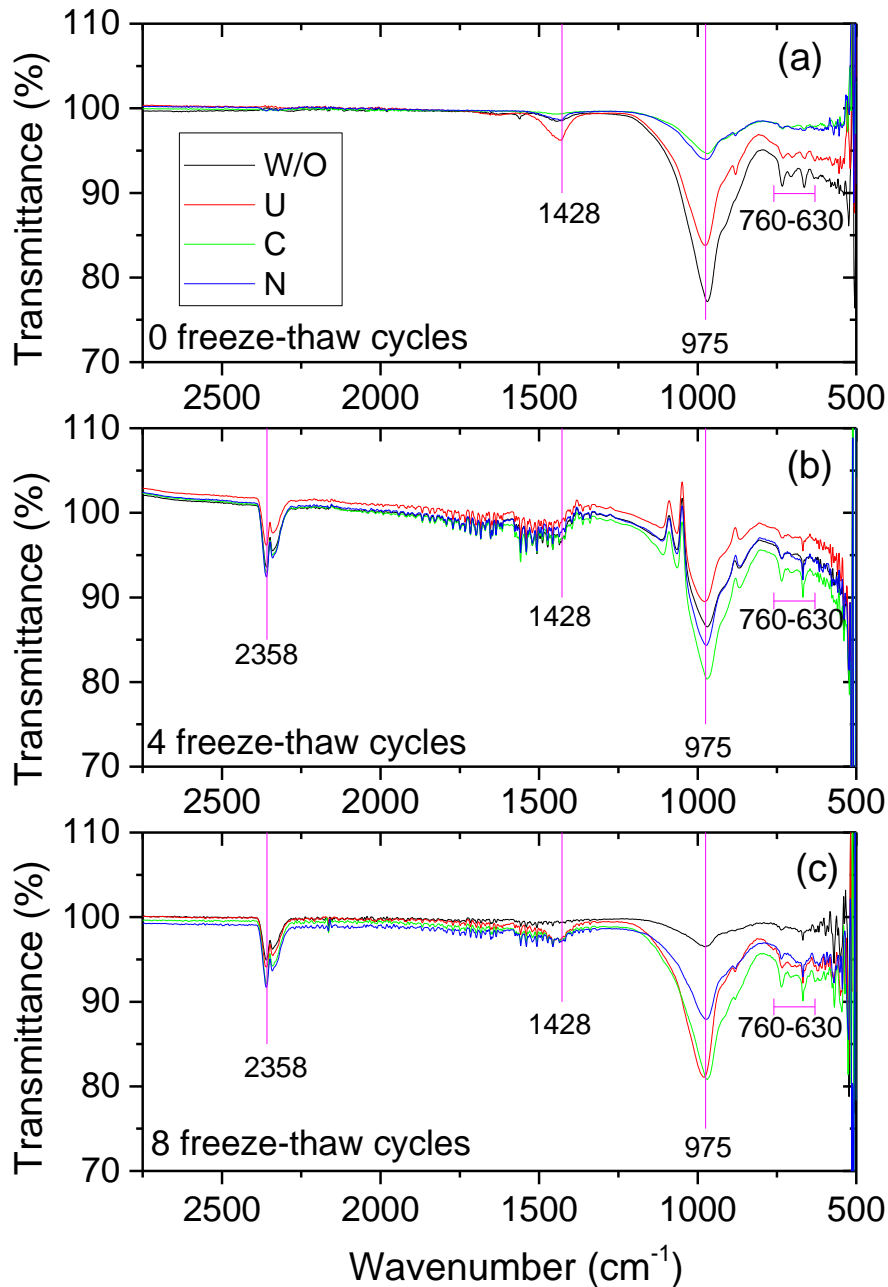


Figure 17. FTIR spectra of lunar Geopolymer specimens containing 0 wt.% superplasticizer (W/O) and 3 wt.% of urea (U), 3% polycarboxylate-based admixture (C), and 3% naphthalene-based admixture (F)(a) after 0 freeze-thaw cycles and (b) after 4 freeze-thaw cycles, and (c) after 8 freeze-thaw cycles.

3.6. X-Ray tomography

Typical 2D X-ray micro-tomography cross-sectional slices obtained from the W/O, U, C, and N samples after 0 and 4 freeze-thaw cycles are shown in **Error! Reference source not found.**, where cracks and air voids are displayed in dark colour (low or no X-ray attenuation). More microcracks are evident in the U matrix after exposure to freeze-thaw cycles. This indicates that the microcracks generated by the freeze-thaw cycles can contribute to the deterioration of the U sample. This is probably a contributing factor to the lower compressive strength of this sample after the freeze thaw cycles (Figure 16).

Error! Reference source not found. illustrates the air voids (in red color) in the 3D images of the samples. In order to quantify the differences, pore diameter distributions are plotted in **Error! Reference source not found.** and the volume fraction, mean diameter, and number of air voids per mm^3 is shown in Figure 21. **Error! Reference source not found.** and Figure 21a illustrate that before the freeze-thaw cycles the inclusion of urea (U) and the polycarboxylate-based admixture (C) led to a substantial increase of porosity in comparison with the sample without any admixture (W/O). This is expected to affect the mechanical performance of the materials, and might be contributing to the lower compressive strength of the U and C samples compared to the W/O sample (Figure 16). A lower flowability or higher viscosity is expected to increase the air content of the mixtures [57]. Accordingly, before the freeze-thaw cycles the better workability of the N sample leads to smaller (**Error! Reference source not found.**, Figure 21 b) and lower amounts (Figure 21a) of air voids compared to the C sample. When aqueous solutions of urea are heated up to 80 °C, NH_3 and H_2 gases can be released [58]. These gases might contribute to creating more voids in the U sample compared to the other samples, as observed in **Error! Reference source not found.** and Figure 21a. Despite its poor workability, the W/O sample has a low amount of air voids before the freeze-thaw cycles compared to the other samples (**Error! Reference source not found.**, Figure 21a). This might indicate that the inclusion of superplasticizers enhances air void formation which provide durability for the sample in freezing-thawing situations [59]. In addition, the mean diameter (Figure 21b) and pore size distribution (**Error! Reference source not found.**) illustrates that larger air voids are formed before the freeze-thaw cycles for the W/O and C samples compared to the N sample. This might suggest that poorer workability of the samples causes the formation of larger air voids [57], [60].

After 4 freeze-thaw cycles, the total volume of air voids increases significantly for the W/O and C samples while there is little change for the U and N samples (**Error! Reference source not found.**, Figure 21a). Accordingly, the differences in compressive strength after the freeze-thaw process (Figure 16) does not seem to be directly correlated with the volume of new air voids formed. This suggests that the effect of the superplasticizers on the geopolymerisation reaction plays a larger role than the formation of additional air voids after the freeze-thaw cycles. As can be seen from **Error! Reference source not found.**, the freeze-thaw cycles seem to shift the size distributions towards larger air voids. This can both be due to an enlargement of existing voids by expansion of entrapped water, and several smaller voids expanding into a common much larger void. The latter effect seems to be dominant for the N-sample, which has significantly fewer voids after the freeze-thaw cycles (Figure 21c).

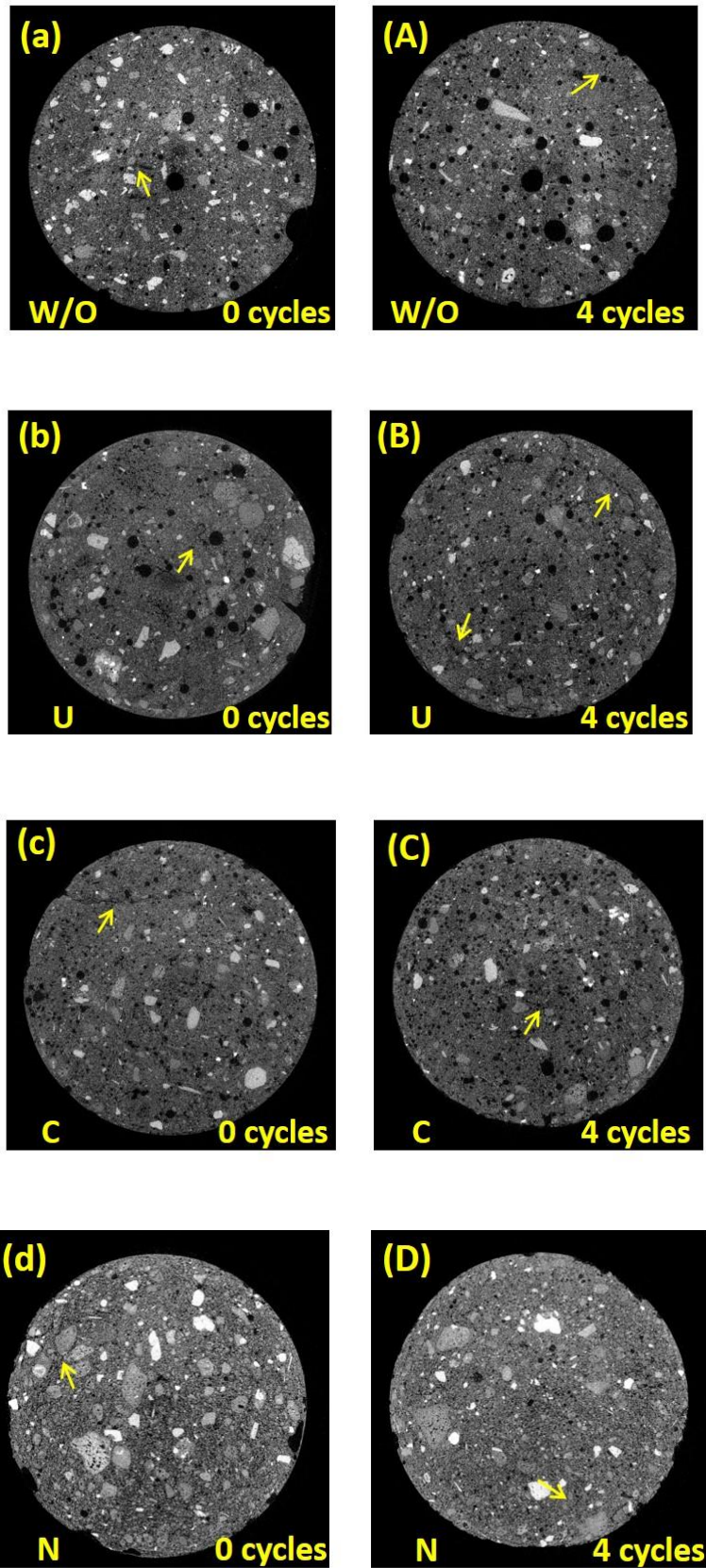


Figure 18. 2D X-ray tomography images of (a) W/O sample – 0 cycles, (A) W/O sample – 4 cycles, (b) U sample – 0 cycles, (B) U sample – 4 cycles, (c) C sample – 0 cycles, (C) C sample – 4 cycles, (d) N sample – 0 cycles, and (D) N sample – 4 cycles. The arrows show the microcracks in the sample matrix. The field of view is approximately 1 cm.

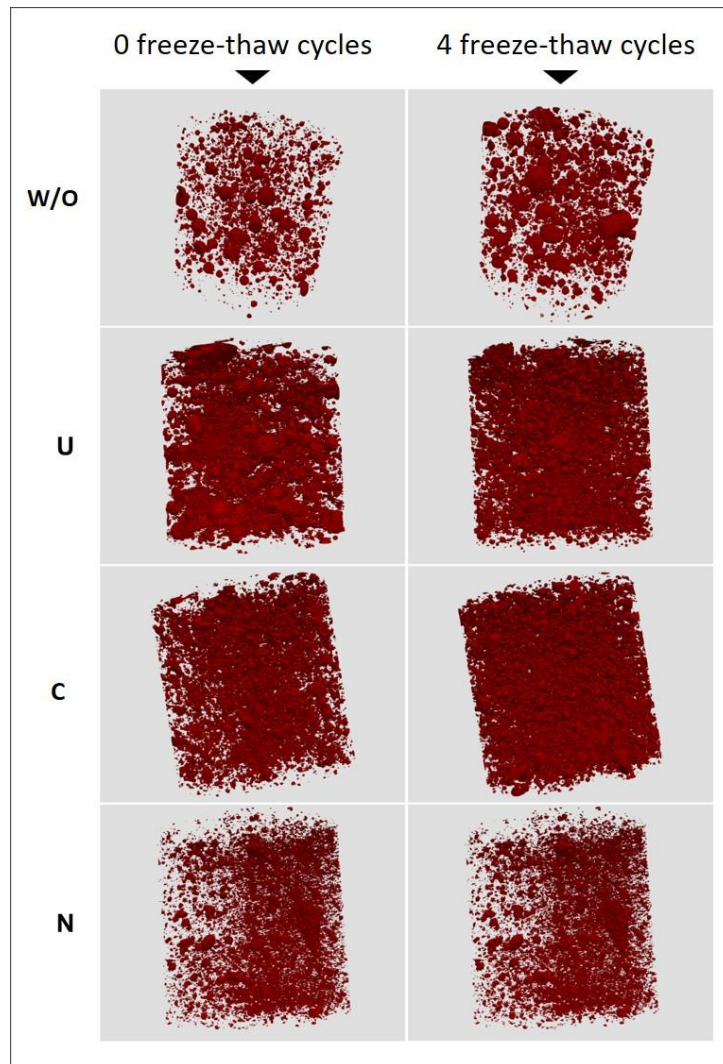


Figure 19. 3D X-ray-tomography rendering of samples containing 0 wt.% superplasticizer (W/O) and 3 wt.% urea (U), 3 wt.% polycarboxylate-based admixture (C), and 3 wt.% naphthalene-based admixture (N) after 0 and 4 freeze-thaw cycles.

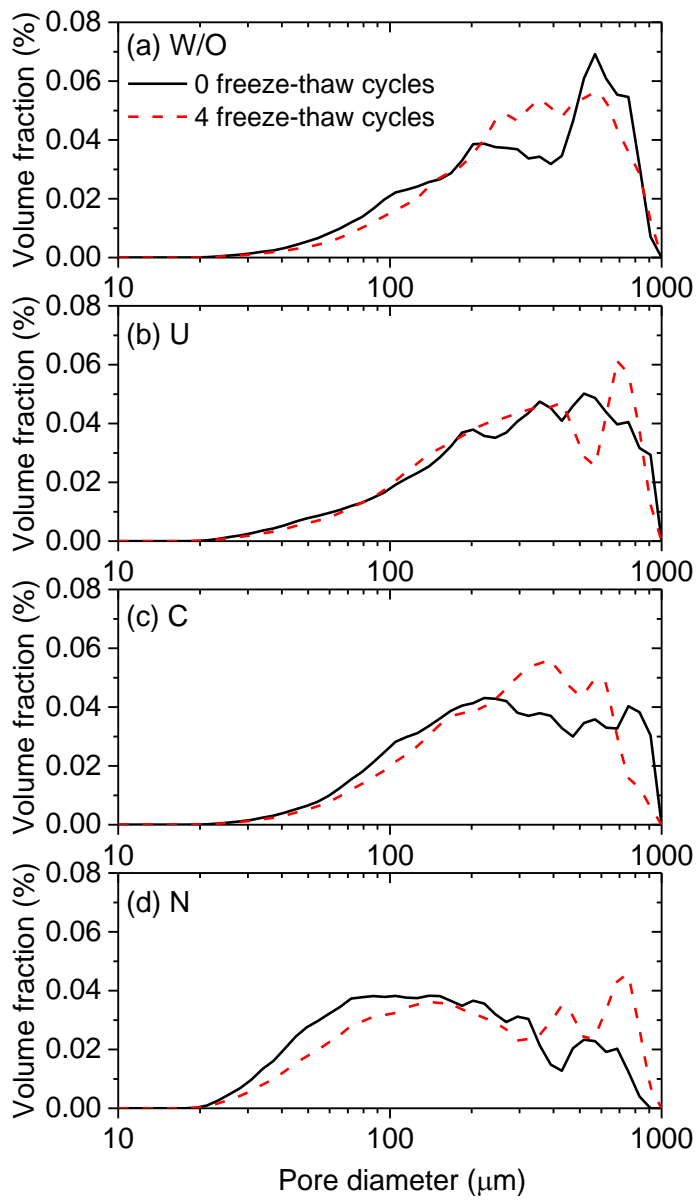


Figure 20. Differential size distributions of air voids inside the W/O, U, C and N samples, obtained from image analyses of the X-ray-tomography images after 0 freeze-thaw cycles and 4 freeze-thaw cycles.

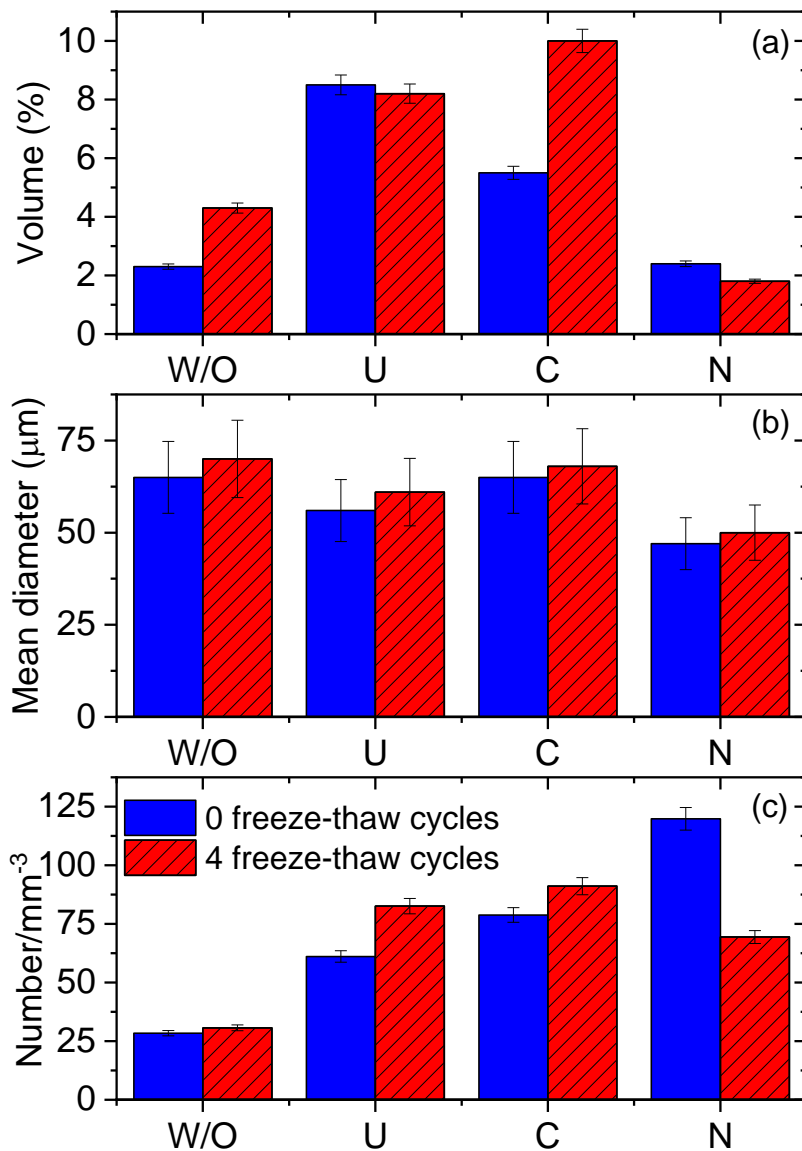


Figure 21. (a) Volume % of air voids, (b) mean diameter of air voids, and (c) number of air voids per mm³ for the W/O, U, C and N samples obtained from image analyses of the X-ray-tomography images after 0 freeze-thaw cycles and 4 freeze-thaw cycles.

3.7. Compressive strength of basalt fibre-reinforced mixes

The average compressive strength of cube samples cured in vacuum condition is shown in Figure 22. It can be observed that the addition of basalt fibre had a negative effect on the compressive strength of lunar geopolymer mixes. Based on the test results, adding 1% short basalt fibres reduced the compressive strength by about 34% compared to that of the control mix. The adverse effect of fibre reinforcement on the compressive strength was more pronounced in mix with 1% long basalt fibres. As observed in the figure, the compressive strength of mix LG-LBF-V was negligible, which indicates that long basalt fibres can weaken the geopolymer matrix significantly. The inferior compressive strength of fibre-reinforced mixes compared to that of the control mix can be related to the lower workability caused by the friction between fibres and geopolymer paste, which prevented proper compaction of the samples. As a result, a less dense geopolymer matrix was formed and the compressive strength was reduced. Furthermore, long basalt fibres can reduce the mobility of the

fresh mix more than short basalt fibres due to their larger aspect ratio, which can be the reason behind the lower compressive strength of LG-LBF-V compared to that of LG-SBF-V.

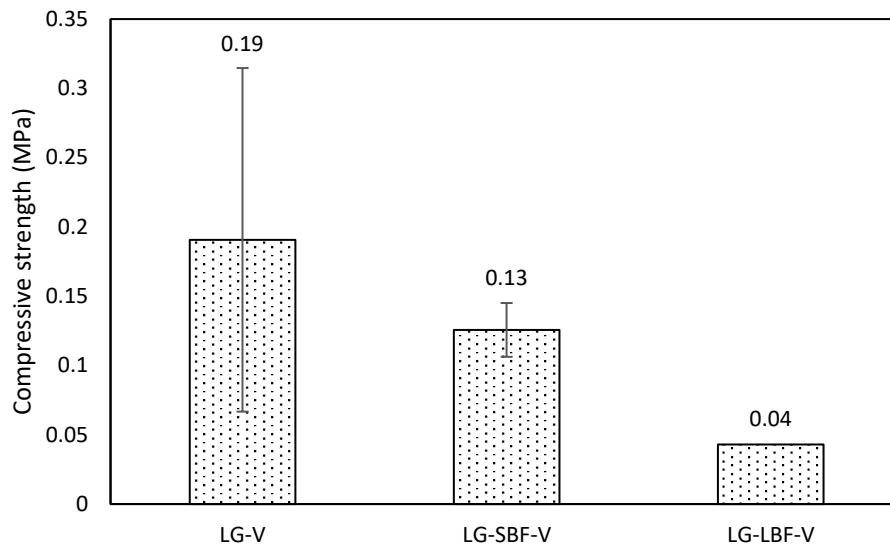


Figure 22. Compressive strength of lunar geopolymer samples cured in vacuum condition.

3.8. Flexural strength of basalt fibre-reinforced mixes

Figure 23 shows the average flexural load-deformation curves of lunar geopolymer mixes. According to this figure, applying 1% basalt fibre enhanced the flexural behavior of mixes significantly. As it can be observed, the control mix demonstrated a brittle behavior and the specimen showed a sudden failure once the maximum flexural strength was achieved. On the other hand, fibre-reinforced mixes showed a ductile behavior and the ultimate deformation was significantly higher than that of the control mix for both LG-SBF-V and LG-LBF-V mixes. Furthermore, the load-bearing capacity of the fibre-reinforced mixes was also higher than that of the control mix. According to Table 6, the average ultimate load sustained by the specimens made with 1% short basalt fibre and 1% long basalt fibre was approximately 16% and 69% higher than that of the control mix, respectively. Basalt fibres could bridge over the micro-cracks, and thereby contributed to the flexural strength of lunar geopolymer mixes. Furthermore, the additional strength provided by the fibre-matrix bond could be another reason behind the superior flexural behavior of fibre-reinforced mixes compared to that of the control mix. The higher load bearing capacity of LG-LBF-V compared to LG-SBF-V could be attributed to the higher friction force provided by the longer basalt fibres compared to short basalt fibres. However, the short basalt fibres could disperse more uniformly in the mixture, and therefore could sew more micro-cracks throughout the specimen. This may justify the higher deformation capacity of mix with short basalt fibres compared to mix with long basalt fibres. Moreover, the area under the load-deformation curve indicates the amount of the absorbed energy. Although the ultimate load resisted by mix LG-SBF-V was lower than that of LG-LBF-V, it absorbed a higher amount of energy, which is due its higher deformation capacity. As presented in Table 6, the average energy absorbed by mix LG-SBF-V was 2.42, while that of mix LG-LBF-V was 2.04.

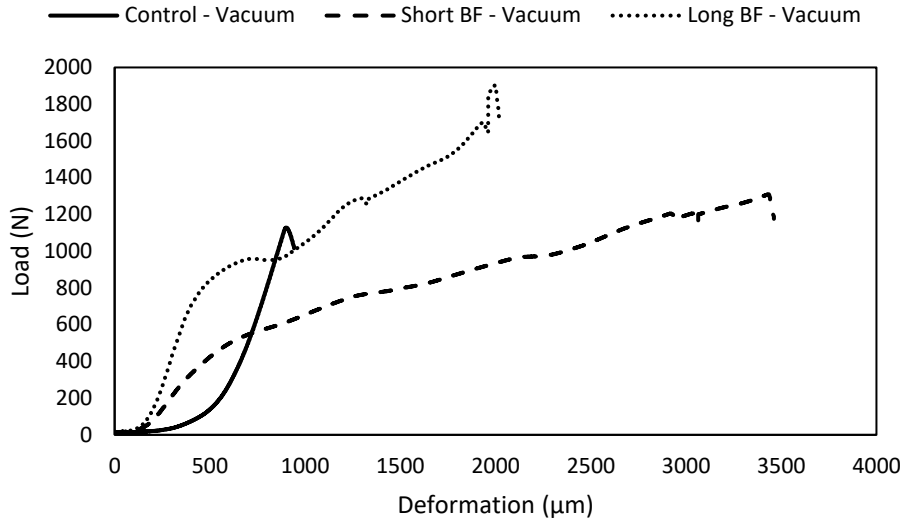


Figure 23. Flexural load-deformation curves of lunar geopolymer mixes cured in vacuum condition.

Table 6. Properties of geopolymer mixes under flexural loading.

Mix	Average ultimate load (N)	Average ultimate deformation (μm)	Average energy (J)
LG-V	1128	941	0.287
LG-SBF-V	1310	3461	2.045
LG-LBF-V	1904	2021	2.42

3.9. Radiation experiments

Radiation experiments were carried out remotely due to the COVID-19 pandemic over a period of 3 days. Experiments were run for one hour per test and a neutron count was measured before and after transmission through the sample. A high threshold was applied to each detector count to reduce noise. Transmission is given as the ratio of neutrons detected after and before the sample. As global count varies between experiments, and to account for environmental attenuation between the two detectors, the transmission is normalised to the neutron count of a blank measurement, i.e., when no sample is present. In order to represent all samples on the same graph, transmission is plotted against interaction depth. The interaction depth is calculated by integrating the density of the shielding material by the sample thickness.

The results in Figure 24 show that the neutron transmission through the shielding material exhibits exponential decay with increasing sample thickness. The dispersion of data points is low, suggesting that there is very little difference in the neutron shielding properties of each sample type. This is to be expected as the shielding property is primarily affected by the chemistry of the shielding material. In the case of reinforced material, the elemental makeup of basalt fibre is highly similar to lunar regolith, which makes up a primary constituent of geopolymer. This, paired with the low volumetric percentage of basalt fibre reinforcement in the material, means that the fibre additions do not provide any changes to shielding effectiveness.

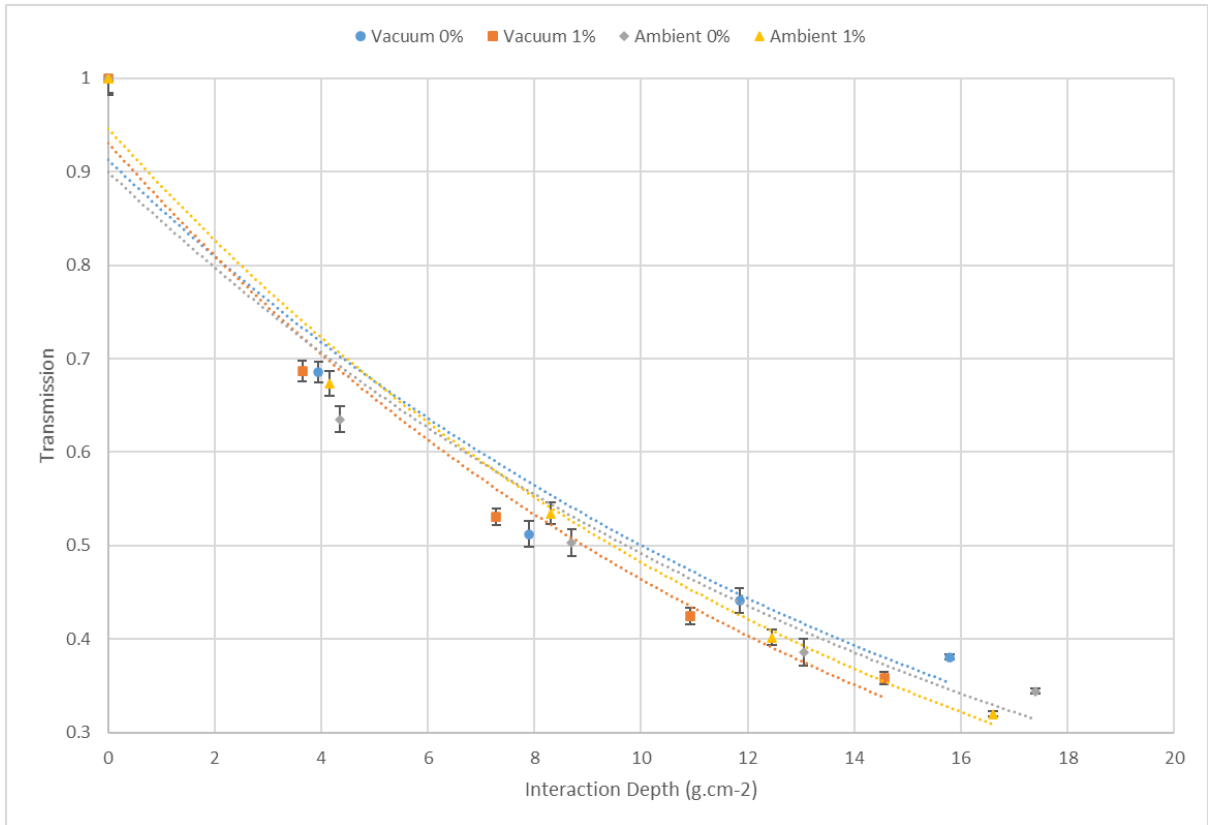


Figure 24. Neutron transmission plotted against interaction depth for the four sample types investigated in this radiation study.

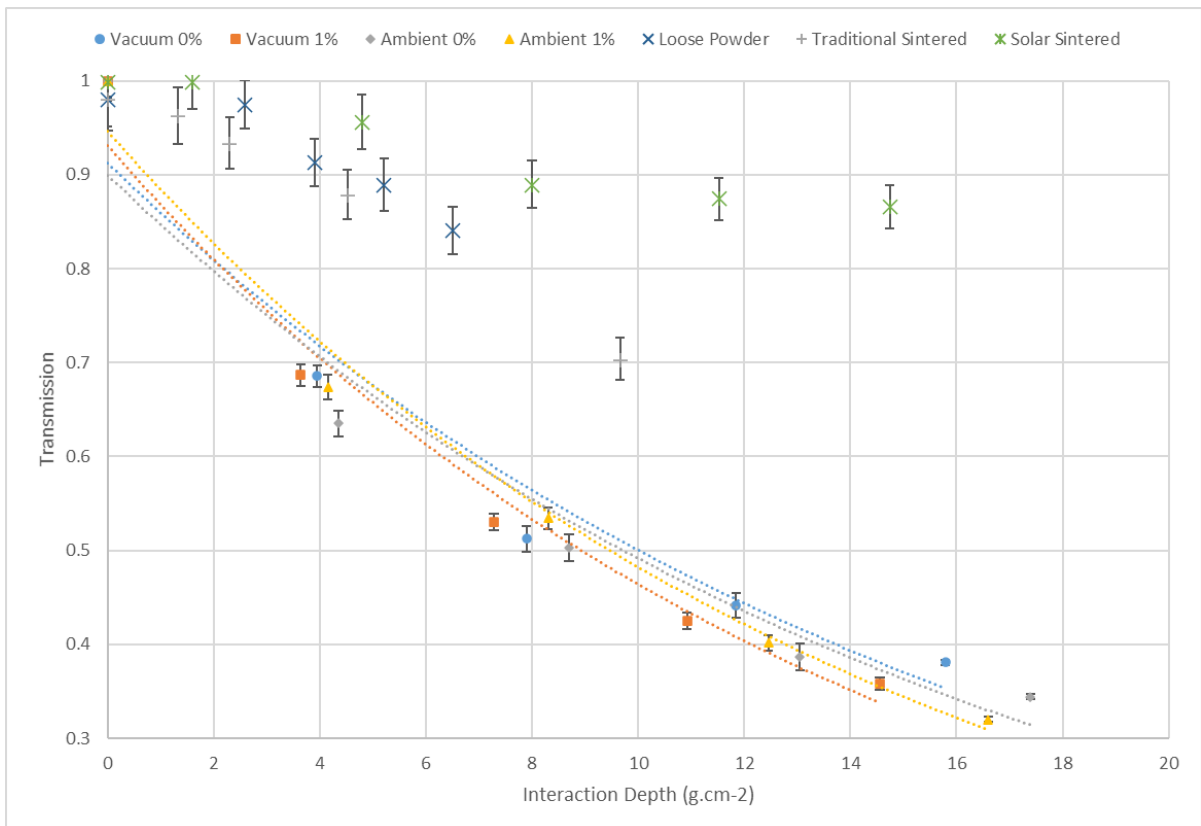


Figure 25. Neutron transmission plotted against interaction depth for the four geopolymer types, compared with three additional materials as investigated by Meurisse et al [49]: loose JSC-2A simulant powder, traditionally sintered simulant and solar sintered simulant.

Meurisse et al. [49] also investigated the neutron shielding properties of lunar regolith materials using a similar experimental setup. The study utilised regolith simulant JSC-2A, which has the same composition as JSC-1A simulant and is similar in composition to DNA-1A simulant (Table 1), and investigated three simulant-based materials: solar sintered regolith, regolith sintered under vacuum using traditional (i.e. non-solar) methods, and loose regolith powder. Figure 25 compares the results of the investigation by Meurisse et al. with the results from the current study. It is clear that the neutron transmission in geopolymer materials is much lower than that of the consolidated or loose regolith. This can be attributed to the increased presence of low atomic number elements in geopolymer, from urea and sodium hydroxide additives. These elements have a high scattering cross section and incident neutrons are more likely to interact with them [61]. Thus, both reinforced and unreinforced geopolymers exhibit greater neutron radiation shielding, irrespective of curing condition, than sintered regolith or loose regolith alone.

4. Conclusions

Future long-term missions to the lunar surface rely on the construction of habitat structures capable of shielding astronauts and equipment from the environment of space. Developing an ISRU-based method to produce such infrastructure will provide immense cost benefits to lunar missions, and thus it is crucial to understand the influence of lunar material and the effects of the space environment on the construction process. This study assessed the feasibility of in-situ lunar geopolymer, first by optimising the geopolymer recipe for use with urea admixture, then comparing the properties of lunar geopolymer cured under ambient conditions to samples cured under simulated lunar conditions (temperature cycling and vacuum). The study also investigated the radiation shielding properties of the material, and assessed the impact of basalt fibre additions on material properties.

- Geopolymers were successfully created using lunar regolith simulant as the geopolymer binder. An optimal recipe was designed for in-situ 3D-printing applications, balancing sufficient workability, low viscosity and minimal water content. This was found to be a NaOH solution to regolith ratio of 0.35, with 3 wt.% superplasticiser (where wt.% is in relation to the binder weight). Samples prepared with urea exhibited greater shape retention under loading and superior buildability pre-curing over sample prepared with traditional superplasticisers, or with no superplasticiser. Urea additions also reduced water demand in the recipe by up to 32%.
- During freeze-thaw cycles, two opposing mechanisms are affecting the compressive strength of geopolymer samples: expansion of water during freezing reduces compressive strength due to fracturing, whilst the continuing geopolymerisation reaction within the samples increases the compressive strength. This resulted in a continuous slight net increase in compressive strength for urea geopolymers, and a final compression strength above the structural requirements for lunar construction (>7 MPa)
- 1% basalt fibre additions enhanced the flexural behaviour of the geopolymer samples significantly. Fibre-reinforced geopolymer mixes showed a ductile behaviour, and showed higher load-bearing capacity and significantly higher ultimate deformation than that of the control mix without fibres for both short and long chopped fibre mixes. The average ultimate load sustained by the specimens made with 1% short basalt fibre and 1% long basalt fibre was approximately 16% and 69% higher than that of the control mix, respectively. Superior flexural performance is associated with microcrack bridging and fibre-matrix bonding. Higher load bearing capacity is associated with friction of fibre pull-out, coupled with high distribution of

fibres for short fibre samples in particular. However, fibre additions were shown to reduce compressive strength by approximately 34% compared to control mixtures.

Radiation tests of the neutron transmission through the geopolymer material show exponential decay with increasing sample thickness. The dispersion of data points is low, suggesting that there is very little difference in the neutron shielding properties of each sample type (i.e. samples with and without fibre addition, samples cured under different environmental conditions). The fibre additions do not provide any changes to shielding effectiveness. The neutron transmission in geopolymer materials is much lower than that of consolidated (sintered) or loose regolith. This can be attributed to the increased presence of low atomic number elements in geopolymer, from urea and sodium hydroxide additives. Thus, both reinforced and unreinforced geopolymers exhibit greater neutron radiation shielding, irrespective of curing condition, than sintered regolith or loose regolith alone.

4.1. Future Work

A 3D-extrusion assembly to test additive manufacturing of the lunar geopolymer in a vacuum chamber was constructed and is currently in the verification stage (Section 2.4). The aim is to use this assembly to investigate the effects of the lunar environment, in particular vacuum, on 3D-printing of geopolymer structures on the surface of the Moon. In addition, further experiments on radiation shielding properties of lunar regolith geopolymers are planned for the near future.

Acknowledgements

The team would like to thank Carlo Cazzaniga and Maria Kastriotou at the ISIS Neutron and Muon Facility for their assistance in conducting radiation experiments on the investigators' behalf.

References

- [1] J. A. Happel, "Indigenous Materials for Lunar Construction," *Appl. Mech. Rev.*, vol. 46, no. 6, pp. 313–325, Jun. 1993, doi: 10.1115/1.3120360.
- [2] S. Benvenuti, F. Ceccanti, and X. De Kestelier, "Living on the Moon: Topological Optimization of a 3D-Printed Lunar Shelter," *Nexus Netw. J.*, vol. 15, no. 2, pp. 285–302, Aug. 2013, doi: 10.1007/s00004-013-0155-7.
- [3] G. Cesaretti, E. Dini, X. De Kestelier, V. Colla, and L. Pambaguian, "Building components for an outpost on the Lunar soil by means of a novel 3D printing technology," *Acta Astronaut.*, vol. 93, pp. 430–450, Jan. 2014, doi: 10.1016/j.actaastro.2013.07.034.
- [4] C. Buchner, R. H. Pawelke, T. Schlauf, A. Reissner, and A. Makaya, "A new planetary structure fabrication process using phosphoric acid," *Acta Astronaut.*, vol. 143, pp. 272–284, Feb. 2018, doi: 10.1016/j.actaastro.2017.11.045.
- [5] E. H. Hauri, A. E. Saal, M. J. Rutherford, and J. A. Van Orman, "Water in the Moon's interior: Truth and consequences," *Earth Planet. Sci. Lett.*, vol. 409, pp. 252–264, Jan. 2015, doi: 10.1016/j.epsl.2014.10.053.
- [6] R. N. Grugel and H. Toutanji, "Sulfur 'concrete' for lunar applications – Sublimation concerns," *Adv. Space Res.*, vol. 41, no. 1, Art. no. 1, Jan. 2008, doi: 10.1016/j.asr.2007.08.018.
- [7] R. N. Grugel, "Sulfur 'Concrete' for Lunar Applications - Environmental Considerations," NASA/TM-2008-215250, Feb. 2008. Accessed: Oct. 31, 2021. [Online]. Available: <https://ntrs.nasa.gov/citations/20080022947>

- [8] H. A. Toutanji, S. Evans, and R. N. Grugel, "Performance of lunar sulfur concrete in lunar environments," *Constr. Build. Mater.*, vol. 29, pp. 444–448, Apr. 2012, doi: 10.1016/j.conbuildmat.2011.10.041.
- [9] D. Hardjito, C. C. Cheak, and C. H. L. Ing, "Strength and Setting Times of Low Calcium Fly Ash-based Geopolymer Mortar," *Mod. Appl. Sci.*, vol. 2, no. 4, pp. 3–11, Jul. 2008.
- [10] Z. Li, Z. Ding, and Y. Zhang, "DEVELOPMENT OF SUSTAINABLE CEMENTITIOUS MATERIALS," presented at the Proceedings of the International Workshop on Sustainable Development and Concrete Technology American Concrete Institute International, Northwestern University, Iowa State University, Changjiang Water Resources Commission, China Building Material Academy, 2004. Accessed: Oct. 31, 2021. [Online]. Available: <https://trid.trb.org/view/741558>
- [11] Y. Fu, L. Cai, and W. Yonggen, "Freeze–thaw cycle test and damage mechanics models of alkali-activated slag concrete," *Constr. Build. Mater.*, vol. 25, no. 7, pp. 3144–3148, Jul. 2011, doi: 10.1016/j.conbuildmat.2010.12.006.
- [12] P. Sun and H.-C. Wu, "Chemical and freeze–thaw resistance of fly ash-based inorganic mortars," *Fuel*, vol. 111, pp. 740–745, Sep. 2013, doi: 10.1016/j.fuel.2013.04.070.
- [13] T. Bakharev, "Durability of geopolymer materials in sodium and magnesium sulfate solutions," *Cem. Concr. Res.*, vol. 35, no. 6, pp. 1233–1246, Jun. 2005, doi: 10.1016/j.cemconres.2004.09.002.
- [14] T. Bakharev, "Resistance of geopolymer materials to acid attack," *Cem. Concr. Res.*, vol. 35, no. 4, pp. 658–670, Apr. 2005, doi: 10.1016/j.cemconres.2004.06.005.
- [15] T. W. Cheng and J. P. Chiu, "Fire-resistant geopolymer produced by granulated blast furnace slag," *Miner. Eng.*, vol. 16, no. 3, pp. 205–210, Mar. 2003, doi: 10.1016/S0892-6875(03)00008-6.
- [16] D. L. Y. Kong and J. G. Sanjayan, "Effect of elevated temperatures on geopolymer paste, mortar and concrete," *Cem. Concr. Res.*, vol. 40, no. 2, pp. 334–339, Feb. 2010, doi: 10.1016/j.cemconres.2009.10.017.
- [17] A. M. Fernandez-Jimenez, A. Palomo, and C. Lopez-Hombrados, "Engineering Properties of Alkali-Activated Fly Ash Concrete," *Mater. J.*, vol. 103, no. 2, pp. 106–112, Mar. 2006, doi: 10.14359/15261.
- [18] C. Montes *et al.*, "Evaluation of lunar regolith geopolymer binder as a radioactive shielding material for space exploration applications," *Adv. Space Res.*, vol. 56, no. 6, pp. 1212–1221, Sep. 2015, doi: 10.1016/j.asr.2015.05.044.
- [19] M. Matta, S. Smith, J. Baumgardner, J. Wilson, C. Martinis, and M. Mendillo, "The sodium tail of the Moon," *Icarus*, vol. 204, no. 2, pp. 409–417, Dec. 2009, doi: 10.1016/j.icarus.2009.06.017.
- [20] R. A. Buswell, W. R. Leal de Silva, S. Z. Jones, and J. Dirrenberger, "3D printing using concrete extrusion: A roadmap for research," *Cem. Concr. Res.*, vol. 112, pp. 37–49, Oct. 2018, doi: 10.1016/j.cemconres.2018.05.006.
- [21] F. Ceccanti, E. Dini, X. D. Kestelier, V. Colla, and L. Priami, "3D printing technology for a moon outpost exploiting lunar soil," *undefined*, 2010, Accessed: Oct. 31, 2021. [Online]. Available: <https://www.semanticscholar.org/paper/3D-printing-technology-for-a-moon-outpost-lunar-Ceccanti-Dini/78f66c145c88aa691152d8056750dea3151806f8>
- [22] T. D. Ngo, A. Kashani, G. Imbalzano, K. T. Q. Nguyen, and D. Hui, "Additive manufacturing (3D printing): A review of materials, methods, applications and challenges," *Compos. Part B Eng.*, vol. 143, pp. 172–196, Jun. 2018, doi: 10.1016/j.compositesb.2018.02.012.

- [23] T. T. Le, S. A. Austin, S. Lim, R. A. Buswell, A. G. F. Gibb, and T. Thorpe, "Mix design and fresh properties for high-performance printing concrete," *Mater. Struct.*, vol. 45, no. 8, pp. 1221–1232, Aug. 2012, doi: 10.1617/s11527-012-9828-z.
- [24] K. M. Chua and S. W. Johnson, "Martian and Lunar Cold Region Soil Mechanics Considerations," *J. Aerosp. Eng.*, vol. 11, no. 4, pp. 138–147, Oct. 1998, doi: 10.1061/(ASCE)0893-1321(1998)11:4(138).
- [25] A. A. Aliabdo, A. E. M. Abd Elmoaty, and H. A. Salem, "Effect of water addition, plasticizer and alkaline solution constitution on fly ash based geopolymer concrete performance," *Constr. Build. Mater.*, vol. 121, pp. 694–703, Sep. 2016, doi: 10.1016/j.conbuildmat.2016.06.062.
- [26] J. Xie and O. Kayali, "Effect of superplasticiser on workability enhancement of Class F and Class C fly ash-based geopolymers," *Constr. Build. Mater.*, vol. C, no. 122, pp. 36–42, 2016, doi: 10.1016/j.conbuildmat.2016.06.067.
- [27] J. G. Jang, N. K. Lee, and H. K. Lee, "Fresh and hardened properties of alkali-activated fly ash/slag pastes with superplasticizers," *Constr. Build. Mater.*, vol. 50, pp. 169–176, Jan. 2014, doi: 10.1016/j.conbuildmat.2013.09.048.
- [28] D. F. Putnam, "Composition and Concentrative Properties of Human Urine," McDonnell Douglas Astronautics Company, Huntington Beach, California, NASA Contractor Report NASA CR-1802, Jul. 1971. Accessed: Oct. 31, 2021. [Online]. Available: <https://ntrs.nasa.gov/api/citations/19710023044/downloads/19710023044.pdf>
- [29] R. Usha and T. Ramasami, "Effect of hydrogen-bond-breaking reagent (urea) on the dimensional stability of rat tail tendon (RTT) collagen fibre," 2002, doi: 10.1002/APP.10262.
- [30] J. Branston, S. Das, S. Y. Kenno, and C. Taylor, "Mechanical behaviour of basalt fibre reinforced concrete," *Constr. Build. Mater.*, vol. 124, pp. 878–886, Oct. 2016, doi: 10.1016/j.conbuildmat.2016.08.009.
- [31] D. Pico, A. Lüking, A. Sempere, and T. Gries, "Moon Basalt fibre – preliminary feasibility study," 2017. <https://www.semanticscholar.org/paper/Moon-Basalt-fibre-%E2%80%93-preliminary-feasibility-study-Pico-L%C3%BCking/ac82bf26373a52a52c287828028a64281a55c303> (accessed Oct. 29, 2021).
- [32] J. E. Colwell, S. Batiste, M. Horányi, S. Robertson, and S. Sture, "Lunar surface: Dust dynamics and regolith mechanics," *Rev. Geophys.*, vol. 45, no. 2, 2007, doi: 10.1029/2005RG000184.
- [33] D. S. McKay *et al.*, "The Lunar Regolith," in *Lunar Sourcebook*, Houston, Texas: Cambridge University Press, 1991. Accessed: Oct. 29, 2021. [Online]. Available: https://www.lpi.usra.edu/publications/books/lunar_sourcebook/pdf/Chapter07.pdf
- [34] H. Toutanji, M. R. Fiske, and M. P. Bodiford, "Development and Application of Lunar "Concrete" for Habitats," in *Earth & Space 2006*, League City/Houston, Texas, United States, Mar. 2006, pp. 1–8. doi: 10.1061/40830(188)69.
- [35] V. Aulesa, "Architecture of lunar habitats," in *Exploration and Utilisation of the Moon*, 2000, vol. 462, p. 289.
- [36] V. C. Li and T. Hashida, "Engineering ductile fracture in brittle-matrix composites," *J. Mater. Sci. Lett.*, vol. 12, no. 12, pp. 898–901, Jan. 1993, doi: 10.1007/BF00455611.
- [37] Y. Li and J. Li, "Relationship between fracture area and tensile strength of cement paste with supplementary cementitious materials," *Constr. Build. Mater.*, vol. 79, pp. 223–228, Mar. 2015, doi: 10.1016/j.conbuildmat.2015.01.052.
- [38] J. Atkinson and K. Zacny, "Mechanical Properties of Icy Lunar Regolith: Application to ISRU on the Moon and Mars," pp. 109–120, Nov. 2018, doi: 10.1061/9780784481899.012.

- [39] C. M. Pieters, "Mare basalt types on the front side of the moon: A summary of spectral reflection data.," *Lunar Planet. Sci. Conf. Proc.*, vol. 3, pp. 2825–2849, Jan. 1978.
- [40] L. A. Taylor, A. Patchen, R. G. Mayne, and D.-H. Taylor, "The most reduced rock from the moon, Apollo 14 basalt 14053: Its unique features and their origin," *Am. Mineral.*, vol. 89, no. 11–12, pp. 1617–1624, Nov. 2004, doi: 10.2138/am-2004-11-1205.
- [41] E. Rill and D. Lowry, "Properties of Basalt Fibre Reinforced Geopolymer Composites," presented at the 34th International Conference & Exposition on Advanced Ceramics & Composites, Daytona Beach, Florida, Jan. 2010. doi: 10.13140/2.1.1763.3287.
- [42] M. Hambach and D. Volkmer, "Properties of 3D-printed fibre-reinforced Portland cement paste," *Cem. Concr. Compos.*, vol. 79, pp. 62–70, May 2017, doi: 10.1016/j.cemconcomp.2017.02.001.
- [43] W. A. Campbell, R. S. Marriott, and J. J. Park, "A Compilation of Outgassing Data for Spacecraft Materials.," NATIONAL AERONAUTICS AND SPACE ADMINISTRATION GREENBELT MD GODDARD SPACE FLIG HT CENTER, Sep. 1973. Accessed: Oct. 29, 2021. [Online]. Available: <https://apps.dtic.mil/sti/citations/ADA309557>
- [44] Basaltex, "Basalt basic properties and product portfolio." Basaltex Belgium, Feb. 2020.
- [45] R. B. Malla and K. M. Brown, "Determination of temperature variation on lunar surface and subsurface for habitat analysis and design," *Acta Astronaut.*, vol. 107, pp. 196–207, Feb. 2015, doi: 10.1016/j.actaastro.2014.10.038.
- [46] L. A. Feldkamp, L. C. Davis, and J. W. Kress, "Practical cone-beam algorithm," *JOSA A*, vol. 1, no. 6, pp. 612–619, Jun. 1984, doi: 10.1364/JOSAA.1.000612.
- [47] C. A. Schneider, W. S. Rasband, and K. W. Eliceiri, "NIH Image to ImageJ: 25 years of image analysis," *Nat. Methods*, vol. 9, no. 7, pp. 671–675, Jul. 2012, doi: 10.1038/nmeth.2089.
- [48] A. Meurisse, "Characterisation of solar sintered lunar regolith simulants," ESA/RAL Advanced Manufacturing Laboratory, Internal Test Report HWL-2017-0003, Apr. 2018.
- [49] A. Meurisse, C. Cazzaniga, C. Frost, A. Barnes, A. Makaya, and M. Sperl, "Neutron radiation shielding with sintered lunar regolith," *Radiat. Meas.*, vol. 132, p. 106247, Mar. 2020, doi: 10.1016/j.radmeas.2020.106247.
- [50] B. Panda and M. J. Tan, "Experimental study on mix proportion and fresh properties of fly ash based geopolymer for 3D concrete printing," *Ceram. Int.*, vol. 44, no. 9, pp. 10258–10265, Jun. 2018, doi: 10.1016/j.ceramint.2018.03.031.
- [51] H. Wei, Y. Fan, and Y. Q. Gao, "Effects of Urea, Tetramethyl Urea, and Trimethylamine N-Oxide on Aqueous Solution Structure and Solvation of Protein Backbones: A Molecular Dynamics Simulation Study," *J. Phys. Chem. B*, vol. 114, no. 1, pp. 557–568, Jan. 2010, doi: 10.1021/jp9084926.
- [52] S. Pilehvar, M. Arnhof, R. Pamies, L. Valentini, and A.-L. Kjøniksen, "Utilization of urea as an accessible superplasticizer on the moon for lunar geopolymer mixtures," *J. Clean. Prod.*, vol. 247, p. 119177, Feb. 2020, doi: 10.1016/j.jclepro.2019.119177.
- [53] S. H. Kosmatka, B. Kerkhoff, W. C. Panarese, N. F. MacLeod, and R. J. McGrath, *Design and Control of Concrete Mixtures*. Cement Association of Canada, 2002.
- [54] M. M. A. B. Abdullah, K. Hussin, M. Bnhussain, K. N. Ismail, Z. Yahya, and R. Abdul Razak, "Fly Ash-based Geopolymer Lightweight Concrete Using Foaming Agent," *Int. J. Mol. Sci.*, vol. 13, no. 6, Art. no. 6, Jun. 2012, doi: 10.3390/ijms13067186.

- [55] C. A. Rees, J. L. Provis, G. C. Lukey, and J. S. J. van Deventer, "In Situ ATR-FTIR Study of the Early Stages of Fly Ash Geopolymer Gel Formation," *Langmuir*, vol. 23, no. 17, pp. 9076–9082, Aug. 2007, doi: 10.1021/la701185g.
- [56] C. A. Rees, J. L. Provis, G. C. Lukey, and J. S. J. van Deventer, "Attenuated Total Reflectance Fourier Transform Infrared Analysis of Fly Ash Geopolymer Gel Aging," *Langmuir*, vol. 23, no. 15, pp. 8170–8179, Jul. 2007, doi: 10.1021/la700713g.
- [57] M. Valcuende, E. Marco, C. Parra, and P. Serna, "Influence of limestone filler and viscosity-modifying admixture on the shrinkage of self-compacting concrete," *Cem. Concr. Res.*, vol. 42, no. 4, pp. 583–592, Apr. 2012, doi: 10.1016/j.cemconres.2012.01.001.
- [58] J. M. Jones and A. N. Rollinson, "Thermogravimetric evolved gas analysis of urea and urea solutions with nickel alumina catalyst," *Thermochim. Acta*, vol. 565, pp. 39–45, Aug. 2013, doi: 10.1016/j.tca.2013.04.034.
- [59] B. Łażniewska-Piekarczyk, "The influence of selected new generation admixtures on the workability, air-voids parameters and frost-resistance of self compacting concrete," *Constr. Build. Mater.*, vol. Complete, no. 31, pp. 310–319, 2012, doi: 10.1016/j.conbuildmat.2011.12.107.
- [60] E. Sakai, T. Kasuga, T. Sugiyama, K. Asaga, and M. Daimon, "Influence of superplasticizers on the hydration of cement and the pore structure of hardened cement," *Cem. Concr. Res.*, vol. 36, no. 11, pp. 2049–2053, Nov. 2006, doi: 10.1016/j.cemconres.2006.08.003.
- [61] D. R. McAlister, "Neutron Shielding Materials," PG Research Foundation Inc., Feb. 2016.